Journal of Computational Physics 458 (2022) 111096

Contents lists available at ScienceDirect

Journal of Computational Physics

www.elsevier.com/locate/jcp

Energy-conserving and time-stepping-varying ESAV-Hermite-Galerkin spectral scheme for nonlocal Klein-Gordon-Schrödinger system with fractional Laplacian in unbounded domains ☆

Shimin Guo [a,*], Can Li [b], Xiaoli Li [c], Liquan Mei [a]

[a] School of Mathematics and Statistics, Xi'an Jiaotong University, Xi'an, 710049, China
[b] Department of Applied Mathematics, Xi'an University of Technology, Xi'an, 710049, China
[c] School of Mathematics, Shandong University, Jinan, 250100, China

ARTICLE INFO

Article history:
Received 17 January 2021
Received in revised form 30 November 2021
Accepted 20 February 2022
Available online 4 March 2022

Keywords:
Klein-Gordon-Schrödinger system
Fractional Laplacian
Hermite function
ESAV
Unbounded domains

ABSTRACT

The aim of this paper is to construct a linearized and energy-conserving numerical scheme for nonlocal-in-space Klein-Gordon-Schrödinger system in multi-dimensional unbounded domains $\mathbb{R}^d$ ($d = 1, 2$, and 3), where the nonlocal property of the system is described by the fractional Laplacian. Firstly, we derive the nonlocal energy conversation law of the system. Then, the Hermite-Galerkin spectral method with scaling factor is employed for the spatial approximation. In the form of the exponential scalar auxiliary variable (ESAV) approach, the Crank-Nicolson scheme with adaptive time-stepping is used for the temporal discretization. To adjust the time-stepping, we propose two kinds of time adaptive strategies depending on the time evolution of the considered system. To avoid solving nonlinear algebra system, the nonlinear terms are explicitly treated by the extrapolation technique. The main advantages of proposed numerical scheme are in three aspects: The first one is that the original nonlocal problem is directly solved in the unbounded domains to avoid the errors and singularities introduced by the domain truncation. The second one is that a linearly explicit and energy-conserving scheme is established with constant coefficients. The third one is the high efficiency without sacrificing accuracy when used in conjunction with the adaptive time-stepping strategies. Numerical experiments are given to demonstrate the accuracy, efficiency, and robustness of the proposed algorithm. As the applications of the scheme, we present numerical simulations of the interactions of 2D/3D vector solitons, which can provide a deeper understanding of nonlinear nonlocal processes in the system.

☆ The project is supported by National Key R&D Program of China (2020YFA0713400 and 2020YFA0713401), NSF of China (12171385, 12131014, 11901489, and 11501441), and NSF of ShaanXi Province (2020JQ-008).

* Corresponding author.
E-mail addresses: shiminguo@mail.xjtu.edu.cn (S. Guo), mathlican@xaut.edu.cn (C. Li), xiaolimath@sdu.edu.cn (X. Li), lqmei@mail.xjtu.edu.cn (L. Mei).

https://doi.org/10.1016/j.jcp.2022.111096
0021-9991/

1. Introduction

In this article, we consider the following nonlocal-in-space Klein-Gordon-Schrödinger (KGS) system with Yukawa coupling and fractional Laplacian in $\mathbb{R}^d$

$$\begin{cases} i\dfrac{\partial u}{\partial t} - \dfrac{\kappa_1}{2}(-\Delta)^{\alpha}u + \gamma u v = 0, & \text{in } \mathbb{R}^d \times (0,T], \quad (1)\\ \dfrac{\partial^2 v}{\partial t^2} + \kappa_2(-\Delta)^{\beta}v + \mu^2 v - \gamma|u|^2 = 0, & \text{in } \mathbb{R}^d \times (0,T], \quad (2)\\ u(\mathbf{x},0) = u_0, \ \ v(\mathbf{x},0) = v_0, \ \ \dfrac{\partial v(\mathbf{x},0)}{\partial t} = v_0^{\diamond}, & \text{in } \mathbb{R}^d, \quad (3)\\ \lim\limits_{|\mathbf{x}|\to\infty} u = \lim\limits_{|\mathbf{x}|\to\infty} v = 0, & \text{in } \mathbb{R}^d \times [0,T], \quad (4) \end{cases}$$

where $\mathbf{x} = (x_1, \cdots, x_d) \in \mathbb{R}^d$ with $\mathbb{R} = (-\infty, +\infty)$, $u = u(\mathbf{x}, t)$ and $v = v(\mathbf{x}, t)$ represent the scalar complex-valued nucleon field and real-valued meson field, respectively. In system (1)-(4), i denotes the imaginary unit, i.e., $i^2 = -1$, the parameters α, β satisfy $1/2 < \alpha, \ \beta < 1$, κ_1 and κ_2 are the positive constants, μ is the ratio of mass between a meson and a nucleon, γ is the coupling constant, u_0 is a complex-valued function, v_0 and $v_0^{\diamond}$ are two real-valued functions, the operator $(-\Delta)^{\theta}$ ($\theta = \alpha, \ \beta$) denotes the fractional Laplacian which is defined in (6) in Sec. 2.

When $\alpha, \beta \to 1$, the KGS system (1)-(2) reduces to the classical model describing the interactions between complex neutron field and neutral meson Yukawa in quantum field theory [1,2]. Many important conclusions on the theoretical analysis [9,10] and numerical solutions [11–13] have been discovered for the classical KGS system. Recently, by generalizing the Feynman path integral over the trajectory of the Lévy flight, the fractional quantum field theory has been developed [3–5] to incorporate the concept of an intrinsically nonlocal fractional kinetic energy expressed by the fractional Laplacian [6]. In fact, the type of kinetic energy in Schrödinger-like models plays a fundamental role for the mode states and particularly for the modifications of the parabolic dispersion. Thus, the fractional quantum mechanics is a natural extension of the classical quantum mechanics [14]. Compared with the classical Schrödinger-like equation involving integer-order Laplacian previously used, the theoretical model with fractional Laplacian [6,32] can provide a better accordance with the observation of bright polariton solitons in a semiconductor microcavity [8]. In this sense, as the generalization of the classical fundamental equations in quantum field theory, the models with fractional Laplacian can give rise to intriguingly mathematical descriptions and form the base of fractional quantum mechanics with non-locality [41].

It is necessary to point out that the discontinuity of the paths of Lévy flights in the fractional quantum mechanics predicates that the corresponding fractional Laplacian should be defined in $\mathbb{R}^d$, which reveals the resulting partial differential equations are naturally set in unbounded domains [42]. However, the related investigation on the numerical solutions of such problems is still limited. Generally, there are three kinds of popular approaches for the numerical treatments of the unbounded domains in the practical computations. The first one is based on the domain truncation. However, such method will introduce the errors and nonphysical singularities at the ending points. The second one is to establish the suitable artificial boundary conditions [16], but it is highly nontrivial for the fractional Laplacian [15]. The last option is the use of orthogonal functions defined in unbounded domains [17,18], which has been successfully applied to the partial differential equations (PDEs) with fractional Laplacian in $\mathbb{R}^d$ [19–21]. Based on the Hermite functions, the authors in Ref. [19] proposed the spectral-Galerkin and collocation methods for PDEs with fractional Laplacian in unbounded domains. Later, Guo et al. [20] extended the Hermite-Galerkin spectral method to the distributed-order nonlinear reaction-diffusion equations with fractional Laplacian in multi-dimensional unbounded domains. Using the explicit formulations for the differential matrices, Tang et al. [21] established Hermite collocation method which is robust for nonlinear problems. In Ref. [15], the spectral method using rational basis (or modified mapped Gegenbauer functions) was developed for PDEs involving fractional Laplacian in $\mathbb{R}^d$. Using the generalized Laguerre functions as basis functions, the authors in Ref. [17] developed spectral methods for fractional PDEs on the half line. To improve the accuracy of the spectral methods, the scaling parameters [22] are introduced into the orthogonal functions in the above mentioned works.

On the other hand, just like the classical quantum system, the conservation of the nonlocal energy is an important property for system (1)-(4). In Sec. 3.1, we shall derive the nonlocal energy conservation law of KGS system (1)-(4). Consequently, it is of interest to construct corresponding conservative and efficient numerical schemes. Because of the appearance of the Yukawa coupling terms $\gamma u v$ and $-\gamma|u|^2$, how to efficiently handle the nonlinear parts in system (1)-(4) is a challenging task. Very recently, an interesting method called scalar auxiliary variable (SAV) approach and its various modifications [24–28] have been successfully proposed to deal with the nonlinear parts of the free energy in gradient flows. With the help of SAV technique, we only need to solve decoupled linear system with constant coefficients. It has been shown that the numerical schemes based on the SAV-type approach are not only efficient and easy to implement, but can also capture the physical properties in the models very well. Among the various improvements of SAV approaches, the ESAV approach proposed by Liu and Li [28] has drawn much attention. Compared with the original version of the SAV approach, the new version removes the bounded-from-below restriction of the nonlinear free energy potential. In addition, unlike the SAV approach, schemes based on the ESAV approach retain the original energy of the system.

In the practical computations, if we use a small time-stepping to ensure good approximations of the problem, the computational cost will be increased. In fact, the small time-stepping may be not necessary in the whole calculation process. When the large time step size is used, we can reduce the computational cost but the obtained numerical results may be inaccurate. A good balance between the efficiency and accuracy is the so-called time adaptive method [29,30], where we adopt small time-stepping if the time evolution of the system is quick while we employ large time-stepping when the system is evolving slowly.

In Ref. [40], the authors used Bourgain space method to analyze local and global well-posedness in the sense of low-regularity for KGS system with fractional Laplacian and studied how the well-posedness is affected by the order of fractional Laplacian. As pointed out in Ref. [40], it is interesting to investigate the KGS system with different orders of fractional Laplacian. For the numerical aspects, the numerical solutions of KGS system with fractional Laplacian in bounded domains have been investigated in Refs. [31–34]. To the best of our knowledge, however, there is no work on investigating the numerical scheme for KGS system in *unbounded* domains. In fact, the unboundedness of the spatial domain is one of the essential difficulties in dealing with the multi-dimensional nonlocal model with fractional Laplacian.

Our aim in this paper is to propose a novel ESAV-Hermite-Galerkin spectral scheme for KGS system (1)-(4) to make it efficient and accurate in the sense that

- it does not require the domain truncation for $\mathbb{R}^d$, which reveals that the additional errors and nonphysical singularities at the interface can be avoided;
- it preserves the nonlocal energy conservation laws at the discrete level to exactly capture the crucial physical properties of the model;
- it has the high efficiency by combining with the ESAV approach and adaptive time-stepping strategies because the resulting algebra system is linear and the small uniform time step size is not needed in the whole calculation.

The remainder of the paper is as follows. In Sec. 2, we give some useful properties of fractional Laplacian and Hermite polynomials/functions. In Sec. 3, we first derive the nonlocal energy conservation law of KGS system (1)-(4). Then, we construct the fully discrete scheme. More specifically, the implementations of the scheme are also presented in this section. Numerical simulations including the corroboration of features of the scheme and its applications are carried out in Sec. 4. Finally, some concluding remarks are given in Sec. 5.

2. Fractional Laplacian and Hermite polynomials/functions

In this part, we describe basic properties of fractional Laplacian and review the useful properties of Hermite polynomials/functions which are of importance in the forthcoming algorithm development and analysis.

Let $\mathbb{C}$ be the set of complex numbers, $|\mathbf{x}|_2$ be the l^2-norm of $\mathbf{x}$ in $\mathbb{R}^d$, i.e., $|\mathbf{x}|_2 = \sqrt{x_1^2 + x_2^2 + \cdots + x_d^2}$. We denote the inner product and norm of space $L^2(\mathbb{R}^d)$ by

$$(u(\mathbf{x}), v(\mathbf{x})) = \int_{\mathbb{R}^d} u(\mathbf{x})\overline{v}(\mathbf{x})\mathrm{d}\mathbf{x}, \quad \|u(\mathbf{x})\| = (u(\mathbf{x}), u(\mathbf{x}))^{\frac{1}{2}}, \quad \forall u(\mathbf{x}), v(\mathbf{x}) \in L^2(\mathbb{R}^d),$$

where $\overline{v}(\mathbf{x})$ stands for the complex conjugate of the function $v(\mathbf{x})$. Let μ be a nonnegative integer, denote $H_C^\mu(\mathbb{R}^d)$ and $H_R^\mu(\mathbb{R}^d)$ be the complex- and real-valued Sobolev spaces of functions on $\mathbb{R}^d$, respectively.

As the generalization of the classical Laplace operator $-\Delta$, the fractional Laplace operator $(-\Delta)^\theta$ $(\theta = \alpha, \beta)$ in (1) and (2) is defined by the following explicit formula [23]

$$(-\Delta)^\theta u(\mathbf{x}) = C(d,\theta)\ \text{p.v.} \int_{\mathbb{R}^d} \frac{u(\mathbf{x}) - u(\mathbf{y})}{|\mathbf{x}-\mathbf{y}|^{d+2\theta}}\mathrm{d}\mathbf{y}, \tag{5}$$

where $C(d,\theta) = \dfrac{2^{2\theta}\theta\Gamma(\theta + d/2)}{\pi^{d/2}\Gamma(1-\theta)}$ denotes the normalization constant, the symbol p.v. stands for the Cauchy principal value. Equivalently, the fractional Laplacian can be defined by the Fourier transform [7]

$$(-\Delta)^\theta u(\mathbf{x}) = \mathcal{F}^{-1}[|\boldsymbol{\xi}|_2^{2\theta}\mathcal{F}[u]](\mathbf{x}), \tag{6}$$

where $|\boldsymbol{\xi}|_2^{2\theta}$ is the 2θ-th power of l^2-norm $|\boldsymbol{\xi}|_2$, $\mathcal{F}$ and $\mathcal{F}^{-1}$ represent the Fourier and inverse Fourier transforms, respectively. For the sake of notational convenience, we also denote the Fourier transform of function $u(\mathbf{x})$ by $\widehat{u}(\boldsymbol{\xi})$ hereafter. Obviously, the definition of fractional Laplacian is expressed in the integral form, which reveals its nonlocal structure. In addition, it gives Fourier multiplier by $|\boldsymbol{\xi}|_2^{2\theta}$ in frequency domain. The fractional Laplacian defined in (5) and (6) is a self-adjoint operator, and the following formula plays a fundamental role in establishing the weak form of (1)-(2): For any $u, v \in H_C^\mu(\mathbb{R}^d)$ or $H_R^\mu(\mathbb{R}^d)$, it holds [19]

$$\left((-\Delta)^{\mu}u,\ v\right)=\left((-\Delta)^{\frac{\mu}{2}}u,\ (-\Delta)^{\frac{\mu}{2}}v\right). \tag{7}$$

We now recall the Hermite polynomials/functions defined over the whole line $\mathbb{R}$. The Hermite polynomials $H_{m_s}(x_s)$ $(s=1,\cdots,d,\ m_s=0,1,2,\cdots)$ are orthogonal with respect to the Hermite weight function $\exp(-x_s^2)$, namely,

$$\int_{-\infty}^{+\infty} H_{m_s}(x_s)H_{n_s}(x_s)\exp(-x_s^2)\mathrm{d}x_s=\begin{cases}1, & m_s=n_s,\\ 0, & m_s\neq n_s,\end{cases}$$

and satisfy the following three-term recurrence relation [35]

$$\begin{cases}H_{m_s+1}(x_s)=x_s\sqrt{\dfrac{2}{m_s+1}}H_{m_s}(x_s)-\sqrt{\dfrac{m_s}{m_s+1}}H_{m_s-1}(x_s),\ \ m_s\geq 1,\\ H_0(x_s)=\pi^{-1/4},\ \ H_1(x_s)=\sqrt{2}\pi^{-1/4}x_s.\end{cases} \tag{8}$$

We define a sequence of Hermite functions $\widetilde{H}_{m_s}(x_s;\lambda_s)$ as

$$\widetilde{H}_{m_s}(x_s;\lambda_s)=\sqrt{\lambda_s}e^{-(\lambda_s x_s)^2/2}H_{m_s}(\lambda_s x_s),\ s=1,\cdots,d,$$

where $\lambda_s>0$ is the scaling factor to arrange the distribution of Hermite-Gauss collocation points in $\mathbb{R}$. In view of (8), we obtain the following three-term recurrence relation for $\widetilde{H}_{m_s}(x_s;\lambda_s)$

$$\begin{cases}\widetilde{H}_{m_s+1}(x_s;\lambda_s)=\lambda_s x_s\sqrt{\dfrac{2}{m_s+1}}\widetilde{H}_{m_s}(x_s;\lambda_s)-\sqrt{\dfrac{m_s}{m_s+1}}\widetilde{H}_{m_s-1}(x_s;\lambda_s),\ \ m_s\geq 1,\\ \widetilde{H}_0(x_s;\lambda_s)=\sqrt{\lambda_s}\pi^{-1/4}e^{-(\lambda_s x_s)^2/2},\ \ \widetilde{H}_1(x_s;\lambda_s)=\lambda_s^{3/2}\sqrt{2}\pi^{-1/4}x_s e^{-(\lambda_s x_s)^2/2}.\end{cases} \tag{9}$$

The orthogonality of the Hermite functions $\widetilde{H}_{m_s}(x_s;\lambda_s)$ can be expressed as

$$\int_{-\infty}^{+\infty}\widetilde{H}_{m_s}(x_s;\lambda_s)\widetilde{H}_{n_s}(x_s;\lambda_s)\mathrm{d}x_s=\delta_{m_s n_s}, \tag{10}$$

where $\delta_{m_s n_s}$ is the Dirac Delta symbol.

The Fourier transform of Hermite functions $\widetilde{H}_{m_s}(x_s;\lambda_s)$ plays a key role in the implementation of the scheme, which reads [19]

$$(\widehat{\widetilde{H}_{m_s}(x_s;\lambda_s)})(\xi_s)=\frac{1}{\sqrt{2\pi}}\int_{-\infty}^{+\infty}\widetilde{H}_{m_s}(x_s;\lambda_s)e^{-i\xi_s x_s}\mathrm{d}x_s=(-i)^{m_s}\widetilde{H}_{m_s}\left(\xi_s;\frac{1}{\lambda_s}\right),\ \ i^2=-1. \tag{11}$$

When $\lambda_s=1$, the above formula indicates that the Hermite function $\widetilde{H}_{m_s}(x_s;\lambda_s)$ is the m_s-th eigenfunction of the Fourier transform operator with the corresponding eigenvalue $(-i)^{m_s}$.

For $s=1,2,\cdots,d$, we define the finite dimensional complex- and real-valued function spaces $\widetilde{P}_{C,N,s}$ and $\widetilde{P}_{R,N,s}$ as

$$\widetilde{P}_{C,N,s}=\left\{k_0\widetilde{H}_0(x_s;\lambda_s)+k_1\widetilde{H}_1(x_s;\lambda_s)+\cdots+k_N\widetilde{H}_N(x_s;\lambda_s)\mid k_0,k_1,\cdots,k_N\in\mathbb{C}\right\},$$
$$\widetilde{P}_{R,N,s}=\left\{l_0\widetilde{H}_0(x_s;\lambda_s)+l_1\widetilde{H}_1(x_s;\lambda_s)+\cdots+l_N\widetilde{H}_N(x_s;\lambda_s)\mid l_0,l_1,\cdots,l_N\in\mathbb{R}\right\}.$$

The d-dimensional tensors of $\widetilde{P}_{C,N,s}$ and $\widetilde{P}_{R,N,s}$, denoted respectively by $\widetilde{\mathbb{P}}^d_{C,N}$ and $\widetilde{\mathbb{P}}^d_{R,N}$, are defined by

$$\widetilde{\mathbb{P}}^d_{C,N}=\widetilde{P}_{C,N,1}\otimes\cdots\otimes\widetilde{P}_{C,N,d},\quad \widetilde{\mathbb{P}}^d_{R,N}=\widetilde{P}_{R,N,1}\otimes\cdots\otimes\widetilde{P}_{R,N,d}.$$

The Hermite-Gauss interpolation operator $I_N: C(\mathbb{R}^d)\to\widetilde{\mathbb{P}}^d_{C,N}$ or $\widetilde{\mathbb{P}}^d_{R,N}$ is defined as

$$(I_N u)(\eta_{j_1},\cdots,\eta_{j_d})=u(\eta_{j_1},\cdots,\eta_{j_d}),\ 0\leq j_1,\cdots,j_d\leq N, \tag{12}$$

where $\{\eta_{j_s}\}_{0\leq j_s\leq N}$ are the Hermite-Gauss points in the x_s-direction with respect to the scaling factor λ_s.

When constructing the scheme, we shall use the generalized Hermite polynomials $G_{m_s}(x_s;\lambda_s;\gamma)$ satisfying the following three-term recurrence [36]

$$\begin{cases}G_{m_s+1}(x_s;\lambda_s;\gamma)=2\lambda_s x_s G_{m_s}(x_s;\lambda_s;\gamma)-2b_{m_s}G_{m_s-1}(x_s;\lambda_s;\gamma),\ \ m_s\geq 1,\\ G_0(x_s;\lambda_s;\gamma)=1,\ \ G_1(x_s;\lambda_s;\gamma)=2\lambda_s x_s,\end{cases} \tag{13}$$

where

$$b_{m_s} = \begin{cases} m_s, & m_s \text{ is even}, \\ m_s + \gamma, & m_s \text{ is odd}. \end{cases}$$

The generalized Hermite polynomials $G_{m_s+1}(x_s; \lambda_s; \gamma)$, defined on the infinite domain $\mathbb{R}$, are mutually orthogonal with respect to the weight function $|x_s|_2^{\gamma} \exp(-(\lambda_s x_s)^2)$ $(s = 1, \cdots, d)$. The Plancherel formula of the Fourier transform will also be used subsequently:

$$\int_{\mathbb{R}} \phi \overline{\varphi} \mathrm{d}x_s = \int_{\mathbb{R}} \widehat{\phi}\, \overline{\widehat{\varphi}} \mathrm{d}\xi_s, \quad \forall \phi,\ \varphi \in L^2(\mathbb{R}). \tag{14}$$

3. ESAV-Hermite-Galerkin spectral scheme

In this section, we construct the linearized, energy-conserving, and time-stepping-varying ESAV-Hermite-Galerkin spectral scheme for system (1)-(4) and present its implementation in details.

3.1. Nonlocal energy conservation law

For system (1)-(4), the nonlocal energy conservation law plays a crucial role in further establishing the numerical scheme. However, the related studies are very sparse. Thus, we first derive the nonlocal energy conservation law of system (1)-(4).

Introducing the auxiliary variable $\varphi = \dfrac{\partial v}{\partial t}$, we rewrite the system (1)-(4) as

$$\begin{cases} i\dfrac{\partial u}{\partial t} - \dfrac{\kappa_1}{2}(-\Delta)^{\alpha} u + \gamma u v = 0, & \text{in } \mathbb{R}^d \times (0, T], \quad (15) \\ \dfrac{\partial v}{\partial t} = \varphi, & \text{in } \mathbb{R}^d \times (0, T], \quad (16) \\ \dfrac{\partial \varphi}{\partial t} + \kappa_2(-\Delta)^{\beta} v + \mu^2 v - \gamma |u|^2 = 0, & \text{in } \mathbb{R}^d \times (0, T], \quad (17) \\ u(\mathbf{x}, 0) = u_0,\ \ v(\mathbf{x}, 0) = v_0,\ \ \varphi(\mathbf{x}, 0) = v_0^{\diamond}, & \text{in } \mathbb{R}^d, \quad (18) \\ \lim\limits_{|\mathbf{x}| \to \infty} u = \lim\limits_{|\mathbf{x}| \to \infty} v = 0, & \text{in } \mathbb{R}^d \times [0, T]. \quad (19) \end{cases}$$

Using the formula (7), taking the inner product of (15) with $\dfrac{\partial u}{\partial t}$ and adding with its conjugate, we obtain

$$-\frac{\kappa_1}{2}\frac{\mathrm{d}}{\mathrm{d}t}\|(-\Delta)^{\frac{\alpha}{2}} u\|^2 + \left(\gamma u v, \frac{\partial \overline{u}}{\partial t}\right) + \left(\gamma \overline{u} v, \frac{\partial u}{\partial t}\right) = 0. \tag{20}$$

Then taking the inner product of (16) with $\dfrac{\partial \varphi}{\partial t}$, we have

$$\left(\frac{\partial v}{\partial t}, \frac{\partial \varphi}{\partial t}\right) = \frac{1}{2}\frac{\mathrm{d}}{\mathrm{d}t}\|\varphi\|^2. \tag{21}$$

Computing the inner product of (17) with $\dfrac{\partial v}{\partial t}$, we have

$$\left(\frac{\partial \varphi}{\partial t}, \frac{\partial v}{\partial t}\right) + \frac{\kappa_2}{2}\frac{\mathrm{d}}{\mathrm{d}t}\|(-\Delta)^{\frac{\beta}{2}} v\| + \frac{\mu^2}{2}\frac{\mathrm{d}}{\mathrm{d}t}\|v\| - \gamma\left(|u|^2, \frac{\partial v}{\partial t}\right) = 0. \tag{22}$$

Considering (20)-(22) and the relation $\varphi = \dfrac{\partial v}{\partial t}$, we can deduce the nonlocal energy conservation law of system (1)-(4) in the following form

$$\frac{\mathrm{d}\mathcal{E}[u, v]}{\mathrm{d}t} = 0, \tag{23}$$

where the nonlocal energy $\mathcal{E}[u, v]$ is defined as

$$\mathcal{E}[u, v] = \frac{1}{2}\left[\kappa_1 \left\|(-\Delta)^{\frac{\alpha}{2}} u\right\|^2 + \kappa_2 \left\|(-\Delta)^{\frac{\beta}{2}} v\right\|^2 + \left\|\frac{\partial v}{\partial t}\right\|^2 + \mu^2 \|v\|^2\right] + \mathcal{E}_1[u, v]. \tag{24}$$

The expression of $\mathcal{E}_1[u, v]$ in (24) is

$$\mathcal{E}_1[u,v]=-\gamma\int_{\mathbb{R}^d}|u|^2v\mathrm{d}\mathbf{x}. \tag{25}$$

3.2. The fully discrete scheme

Motivated by the idea of ESAV approach, we introduce a scalar auxiliary variable $r(t)=\exp(\mathcal{E}_1)$, and rewrite (15)-(17) as

$$\begin{cases} i\dfrac{\partial u}{\partial t}-\dfrac{\kappa_1}{2}(-\Delta)^{\alpha}u+\dfrac{\gamma r}{\exp(\mathcal{E}_1)}(uv)=0, & \text{in } \mathbb{R}^d\times(0,T], \quad (26)\\ \dfrac{\partial v}{\partial t}=\varphi, & \text{in } \mathbb{R}^d\times(0,T], \quad (27)\\ \dfrac{\partial \varphi}{\partial t}+\kappa_2(-\Delta)^{\beta}v+\mu^2v-\dfrac{\gamma r}{\exp(\mathcal{E}_1)}(|u|^2)=0, & \text{in } \mathbb{R}^d\times(0,T], \quad (28)\end{cases}$$

where $r(t)$ satisfies the following ODE

$$\frac{\mathrm{d}\ln(r(t))}{\mathrm{d}t}=-\frac{\gamma r}{\exp(\mathcal{E}_1)}\int_{\mathbb{R}^d}\left[|u|^2\frac{\partial v}{\partial t}+\overline{u}v\frac{\partial u}{\partial t}+uv\frac{\partial\overline{u}}{\partial t}\right]\mathrm{d}\mathbf{x}. \tag{29}$$

Taking the inner product of (26) with $\dfrac{\partial u}{\partial t}$ and adding with its conjugate, taking the inner products of (27) and (28) with $\dfrac{\partial \varphi}{\partial t}$ and $\dfrac{\partial v}{\partial t}$, respectively, and combining them with (29), we can see the above coupled system satisfies the following nonlocal energy conservation law

$$\frac{\mathrm{d}\widetilde{\mathcal{E}}[u,v,\varphi,r]}{\mathrm{d}t}=0, \tag{30}$$

where the ESAV nonlocal energy $\widetilde{\mathcal{E}}[u,v,\varphi,r]$ is defined as

$$\widetilde{\mathcal{E}}[u,v,\varphi,r]=\frac{1}{2}\left[\kappa_1\|(-\Delta)^{\frac{\alpha}{2}}u\|^2+\kappa_2\|(-\Delta)^{\frac{\beta}{2}}v\|^2+\|\varphi\|^2+\mu^2\|v\|^2\right]+\ln(r). \tag{31}$$

Because $\ln(r)=\ln(\exp(\mathcal{E}_1))=\mathcal{E}_1$ and $\varphi=\dfrac{\partial v}{\partial t}$, we have

$$\widetilde{\mathcal{E}}[u,v,\varphi,r]=\mathcal{E}[u,v],$$

which reveals that the energy defined in (31) is exactly equal to the original energy defined in (24).

Now, we construct the fully discrete scheme for (26)-(29), where the main steps contain the spatial approximation and temporal discretization.

Step 1: Spatial semi-discrete scheme

Based on the formula (7), we reformulate (26)-(29) in the weak form: Find $(u(t),v(t),\varphi(t))\in\widetilde{V}_C\times\widetilde{V}_R\times\widetilde{V}_R$, such that for all $(\chi_1,\chi_2,\chi_3)\in H_C^{\alpha}(\mathbb{R}^d)\times H_R^{\beta}(\mathbb{R}^d)\times H_R^{\beta}(\mathbb{R}^d)$,

$$\begin{cases} i\left(\dfrac{\partial u}{\partial t},\chi_1\right)-\dfrac{\kappa_1}{2}\left((-\Delta)^{\frac{\alpha}{2}}u,(-\Delta)^{\frac{\alpha}{2}}\chi_1\right)+\dfrac{\gamma r}{\exp(\mathcal{E}_1)}(uv,\chi_1)=0,\\ \left(\dfrac{\partial v}{\partial t},\chi_2\right)=(\varphi,\chi_2),\\ \left(\dfrac{\partial \varphi}{\partial t},\chi_3\right)+\kappa_2\left((-\Delta)^{\frac{\beta}{2}}v,(-\Delta)^{\frac{\beta}{2}}\chi_3\right)+\mu^2(v,\chi_3)-\dfrac{\gamma r}{\exp(\mathcal{E}_1)}(|u|^2,\chi_3)=0,\end{cases} \tag{32}$$

where $\widetilde{V}_C=L^2(0,T;H_C^{\alpha}(\mathbb{R}^d))$, $\widetilde{V}_R=L^2(0,T;H_R^{\beta}(\mathbb{R}^d))$, and $r(t)$ satisfies (29).

The semi-discrete approximation gives: Find $(u_N(t),\ v_N(t),\ \varphi_N(t))\in\widetilde{V}_{C,N}\times\widetilde{V}_{R,N}\times\widetilde{V}_{R,N}$, such that for all $(\chi_{1N},\chi_{2N},\chi_{3N})\in\widetilde{\mathbb{P}}_{C,N}^d\times\widetilde{\mathbb{P}}_{R,N}^d\times\widetilde{\mathbb{P}}_{R,N}^d$

$$\begin{cases} i\left(\dfrac{\partial u_N}{\partial t},\chi_{1N}\right)-\dfrac{\kappa_1}{2}\left((-\Delta)^{\frac{\alpha}{2}}u_N,(-\Delta)^{\frac{\alpha}{2}}\chi_{1N}\right)+\dfrac{\gamma r_N}{\exp(\mathcal{E}_1[u_N,v_N])}(u_Nv_N,\chi_{1N})=0, & (33)\\ \left(\dfrac{\partial v_N}{\partial t},\chi_{2N}\right)=(\varphi_N,\chi_{2N}), & (34)\\ \left(\dfrac{\partial \varphi_N}{\partial t},\chi_{3N}\right)+\kappa_2\left((-\Delta)^{\frac{\beta}{2}}v_N,(-\Delta)^{\frac{\beta}{2}}\chi_{3N}\right)+\mu^2(v_N,\chi_{3N})-\dfrac{\gamma r_N}{\exp(\mathcal{E}_1[u_N,v_N])}(|u_N|^2,\chi_{3N})=0, & (35)\end{cases}$$

where $\widetilde{V}_{C,N} = L^2(0,T;\widetilde{\mathbb{P}}^d_{C,N})$, $\widetilde{V}_{R,N} = L^2(0,T;\widetilde{\mathbb{P}}^d_{R,N})$, and $r_N(t)$ satisfies the following ODE

$$\frac{\mathrm{d}\ln(r_N)}{\mathrm{d}t} = -\frac{\gamma r_N}{\exp(\mathcal{E}_1[u_N,v_N])}\int_{\mathbb{R}^d}\left[|u_N|^2\frac{\partial v_N}{\partial t} + \overline{u_N}v_N\frac{\partial u_N}{\partial t} + u_N v_N\frac{\partial \overline{u_N}}{\partial t}\right]\mathrm{d}\mathbf{x}. \tag{36}$$

Step 2: Temporal discretization

Now, we construct the temporal discretization for semi-discrete scheme (33)-(36). At each time level, the temporal derivative is discretized by the Crank-Nicolson scheme with adaptive time-stepping. We define the time step $\tau_n = t_{n+1} - t_n$ with $\zeta_{n+1} = \frac{\tau_{n+1}}{\tau_n}$ the ratio of the adjacent time steps. For the uniform time-stepping, we have $\tau_0 = \tau_1 = \cdots = \tau$ and $\zeta_0 = \zeta_1 = \cdots = 1$. Denote by w^n the approximation of the function $w(\cdot,t_n)$ and denote

$$w^{n+\frac12} = \frac{w^{n+1}+w^n}{2}, \quad \widetilde{w}^{n+\frac12} = \left(1+\frac{\zeta_n}{2}\right)w^n - \frac{\zeta_n}{2}w^{n-1}, \quad \widetilde{\rho}^{n+\frac12} = \frac{\gamma\widetilde{r}_N^{n+\frac12}}{\exp\left(\mathcal{E}_1[\widetilde{u}_N^{n+\frac12},\widetilde{v}_N^{n+\frac12}]\right)}.$$

The fully discrete scheme for (33)-(36) reads: Find $(u_N^{n+1}, v_N^{n+1}, \varphi_N^{n+1}) \in \widetilde{\mathbb{P}}^d_{C,N}\times\widetilde{\mathbb{P}}^d_{R,N}\times\widetilde{\mathbb{P}}^d_{R,N}$ $(n\geq 1)$, such that for all $(\chi_{1N},\chi_{2N},\chi_{3N}) \in \widetilde{\mathbb{P}}^d_{C,N}\times\widetilde{\mathbb{P}}^d_{R,N}\times\widetilde{\mathbb{P}}^d_{R,N}$,

$$\begin{cases} i\left(\dfrac{u_N^{n+1}-u_N^n}{\tau_n},\chi_{1N}\right) - \dfrac{\kappa_1}{2}\left((-\Delta)^{\frac{\alpha}{2}}u_N^{n+\frac12},(-\Delta)^{\frac{\alpha}{2}}\chi_{1N}\right) + \widetilde{\rho}^{n+\frac12}\left(\widetilde{u}_N^{n+\frac12}\widetilde{v}_N^{n+\frac12},\chi_{1N}\right) = 0, & (37)\\ \left(\dfrac{v_N^{n+1}-v_N^n}{\tau_n},\chi_{2N}\right) = \left(\varphi_N^{n+\frac12},\chi_{2N}\right), & (38)\\ \left(\dfrac{\varphi_N^{n+1}-\varphi_N^n}{\tau_n},\chi_{3N}\right) + \kappa_2\left((-\Delta)^{\frac{\beta}{2}}v_N^{n+\frac12},(-\Delta)^{\frac{\beta}{2}}\chi_{3N}\right) + \mu^2\left(v_N^{n+\frac12},\chi_{3N}\right) - \widetilde{\rho}^{n+\frac12}\left(|\widetilde{u}_N^{n+\frac12}|^2,\chi_{3N}\right) = 0, & (39)\end{cases}$$

where r_N^{n+1} satisfies

$$\frac{\ln(r_N^{n+1})-\ln(r_N^n)}{\tau_n} = -\widetilde{\rho}^{n+\frac12}\int_{\mathbb{R}^d}\left[|\widetilde{u}_N^{n+\frac12}|^2\frac{v_N^{n+1}-v_N^n}{\tau_n} + \overline{\widetilde{u}_N^{n+\frac12}}\widetilde{v}_N^{n+\frac12}\frac{u_N^{n+1}-u_N^n}{\tau_n} + \widetilde{u}_N^{n+\frac12}\widetilde{v}_N^{n+\frac12}\frac{\overline{u_N^{n+1}}-\overline{u_N^n}}{\tau_n}\right]\mathrm{d}\mathbf{x}. \tag{40}$$

Clearly, we can calculate u_N^{n+1}, v_N^{n+1}, and φ_N^{n+1} from (37)-(39). Then, from (40), we can update r_N^{n+1} by

$$\begin{aligned} r_N^{n+1} = \exp\Bigg(\ln(r_N^n) - \widetilde{\rho}^{n+\frac12}\int_{\mathbb{R}^d}\Big[&|\widetilde{u}_N^{n+\frac12}|^2(v_N^{n+1}-v_N^n) + \overline{\widetilde{u}_N^{n+\frac12}}\widetilde{v}_N^{n+\frac12}(u_N^{n+1}-u_N^n)\\ &+ \widetilde{u}_N^{n+\frac12}\widetilde{v}_N^{n+\frac12}(\overline{u_N^{n+1}}-\overline{u_N^n})\Big]\mathrm{d}\mathbf{x}\Bigg). \end{aligned} \tag{41}$$

Note that the scheme (37)-(40) is devoted to computing u_N^{n+1}, v_N^{n+1}, φ_N^{n+1}, and r^{n+1} with $n\geq 1$. We compute u_N^1, v_N^1, φ_N^1, and r^1 by the following predictor-corrector scheme. Firstly, we calculate $u_N^{1,0}$, $v_N^{1,0}$, $\varphi_N^{1,0}$, and $r^{1,0}$ by

$$\begin{cases} i\left(\dfrac{u_N^{1,0}-u_N^0}{\tau_0},\chi_{1N}\right) - \dfrac{\kappa_1}{2}\left((-\Delta)^{\frac{\alpha}{2}}\dfrac{u_N^{1,0}+u_N^0}{2},(-\Delta)^{\frac{\alpha}{2}}\chi_{1N}\right) + \dfrac{\gamma r_N^0}{\exp\left(\mathcal{E}_1[u_N^0,v_N^0]\right)}\left(u_N^0v_N^0,\chi_{1N}\right) = 0, & (42)\\ \left(\dfrac{v_N^{1,0}-v_N^0}{\tau_0},\chi_{2N}\right) = \left(\dfrac{\varphi_N^{1,0}+\varphi_N^0}{2},\chi_{2N}\right), & (43)\\ \left(\dfrac{\varphi_N^{1,0}-\varphi_N^0}{\tau_0},\chi_{3N}\right) + \kappa_2\left((-\Delta)^{\frac{\beta}{2}}\dfrac{v_N^{1,0}+v_N^0}{2},(-\Delta)^{\frac{\beta}{2}}\chi_{3N}\right) + \mu^2\left(\dfrac{v_N^{1,0}+v_N^0}{2},\chi_{3N}\right) & (44)\\ \qquad - \dfrac{\gamma r_N^0}{\exp\left(\mathcal{E}_1[u_N^0,v_N^0]\right)}\left(|u_N^0|^2,\chi_{3N}\right) = 0,\\ \dfrac{\ln(r_N^{1,0})-\ln(r_N^0)}{\tau_0} = -\dfrac{\gamma r_N^0}{\exp\left(\mathcal{E}_1[u_N^0,v_N^0]\right)}\displaystyle\int_{\mathbb{R}^d}\left[|u_N^0|^2\frac{v_N^{1,0}-v_N^0}{\tau_0} + \overline{u_N^0}v_N^0\frac{u_N^{1,0}-u_N^1}{\tau_0} + u_N^0v_N^0\frac{\overline{u_N^{1,0}}-\overline{u_N^0}}{\tau_0}\right]\mathrm{d}\mathbf{x}, & (45)\\ u_N^0 = I_Nu_0, \quad v_N^0 = I_Nv_0, \quad \varphi_N^0 = I_Nv_0^\diamond, & (46)\end{cases}$$

Algorithm 1 Time step adaptive procedure based on step function.

Given: the values of u_N^k, v_N^k, φ_N^k, and r_N^k $(k = n-1, n)$; the minimum and maximum time step sizes τ_{min} and τ_{max}; the current time step sizes τ_{n-1}; the parameters tol_{min}, tol_{max}, $0 < q < 1$, and $p > 1$.

1): Compute $e_n = \max\left\{\frac{\|u_N^n - u_N^{n-1}\|}{\|u_N^{n-1}\|}, \frac{\|v_N^n - v_N^{n-1}\|}{\|v_N^{n-1}\|}\right\}$.

2): **if** $e_n > tol_{max}$
Recalculate the time step $\tau_{n-1} = \max\{\tau_{min}, q\tau_{n-1}\}$.
Recalculate u_N^n, v_N^n, φ_N^n, and r_N^n by (37)-(40).
goto **1)**.

3): **elseif** $tol_{min} \le e_n \le tol_{max}$
Set the time step $\tau_n = \tau_{n-1}$.
Compute u_N^{n+1}, v_N^{n+1}, φ_N^{n+1}, and r_N^{n+1} by (37)-(40).

4): **else**
Update the time step $\tau_n = \min\{\tau_{max}, p\tau_{n-1}\}$.
Compute u_N^{n+1}, v_N^{n+1}, φ_N^{n+1}, and r_N^{n+1} by (37)-(40).

5): **endif**

where I_N is the Hermite-Gauss interpolation operator defined in (12). Then, we compute $u_N^1, v_N^1, \varphi_N^1$, and r^1 by

$$\begin{cases} i\left(\frac{u_N^1 - u_N^0}{\tau_0}, \chi_{1N}\right) - \frac{\kappa_1}{2}\left((-\Delta)^{\frac{\alpha}{2}}\frac{u_N^1 + u_N^0}{2}, (-\Delta)^{\frac{\alpha}{2}}\chi_{1N}\right) + \frac{\gamma r_N^\star}{\exp\left(\mathcal{E}_1[u_N^\star, v_N^\star]\right)}\left(u_N^\star v_N^\star, \chi_{1N}\right) = 0, & (47) \\ \left(\frac{v_N^1 - v_N^0}{\tau_0}, \chi_{2N}\right) = \left(\frac{\varphi_N^1 + \varphi_N^0}{2}, \chi_{2N}\right), & (48) \\ \left(\frac{\varphi_N^1 - \varphi_N^0}{\tau_0}, \chi_{3N}\right) + \kappa_2\left((-\Delta)^{\frac{\beta}{2}}\frac{v_N^1 + v_N^0}{2}, (-\Delta)^{\frac{\beta}{2}}\chi_{3N}\right) + \mu^2\left(\frac{v_N^1 + v_N^0}{2}, \chi_{3N}\right) & (49) \\ \quad - \frac{\gamma r_N^\star}{\exp\left(\mathcal{E}_1[u_N^\star, v_N^\star]\right)}\left(|u_N^\star|^2, \chi_{3N}\right) = 0, \\ \frac{r_N^1 - r_N^0}{\tau_0} = -\frac{\gamma r_N^\star}{\exp\left(\mathcal{E}_1[u_N^\star, v_N^\star]\right)}\int_{\mathbb{R}^d}\left[|u_N^\star|^2\frac{v_N^1 - v_N^0}{\tau_0} + \overline{u_N^\star}v_N^\star\frac{u_N^1 - u_N^0}{\tau_0} + u_N^\star v_N^\star\frac{\overline{u_N^1} - \overline{u_N^0}}{\tau_0}\right]d\mathbf{x}, & (50) \end{cases}$$

where $u_N^\star = \frac{u_N^{1,0} + u_N^0}{2}$, $v_N^\star = \frac{v_N^{1,0} + v_N^0}{2}$, and $r_N^\star = \frac{r_N^{1,0} + r_N^0}{2}$.

The adaptive time-stepping strategies can reduce the CPU time in the long time simulation. Thus, it is worth studying the adaptive time-stepping control for the scheme. To measure the rapidity of the time evolution of the system at t_n, we introduce the following indicator

$$e_n = \max\left\{\frac{\|u_N^n - u_N^{n-1}\|}{\|u_N^{n-1}\|}, \frac{\|v_N^n - v_N^{n-1}\|}{\|v_N^{n-1}\|}\right\}, \quad n \ge 1. \tag{51}$$

Next, we shall investigate two control algorithms to update the time-stepping based on the time evolution of the system.

The first one is based on the step function: When the time evolution indicator e_n is larger than threshold tol_{max}, we consider decreasing the current time step size τ_{n-1} by multiplying it by a common ratio $0 < q < 1$ and recalculating the values of u_N^n, v_N^n, φ_N^n, and r_N^n; When $e_n \in [tol_{min}, tol_{max}]$, the time-stepping is neither increased nor decreased, i.e., $\tau_n = \tau_{n-1}$; On the other hand, we update the time step size $\tau_n = p\tau_{n-1}$ with $p > 1$ if $e_n < tol_{min}$. For a better understanding, this adaptive time-stepping algorithm is given in Algorithm 1.

The second option to adaptively select the time-stepping is based on the logarithmic function: The formula for updating the time step size is given by

$$A_{dp}(e, \tau) = \sigma|\log_l(e)|\tau, \tag{52}$$

where $\sigma > 0$ is the safety coefficient, e is the time evolution indicator defined in (51), l is the base number of the logarithmic function. We describe this strategy for updating time-stepping in Algorithm 2.

In Algorithms 1 and 2, we set a minimum time step τ_{min} and maximum time step τ_{max} to avoid using very big and very small time steps. For the given minimum time step τ_{min}, we first calculate the u_N^1, v_{kN}^1, φ_N^1, and r_N^1 by prediction-correction scheme (42)-(50) with $\tau_0 = \tau_{min}$. In our practical computations in Sec. 4, we set $tol_{min} = 5e-3$, $tol_{max} = 1e-1$, $q = 0.8$, and $p = 1.2$ in Algorithm 1 and $\sigma = 0.5$ and $l = 10$ in Algorithm 2. In addition, we set $\tau_{min} = 1e-2$ and $\tau_{max} = 1e-1$ in these two algorithms.

Algorithm 2 Time step adaptive procedure based on logarithmic function.

Given: the values of u_N^k, v_N^k, φ_N^k, and r_N^k $(k = n-1, n)$; the minimum and maximum time step sizes τ_{min} and τ_{max}; the current time step sizes τ_{n-1}; the parameters σ and l.

1): Compute $e_n = \max\left\{\frac{\|u_N^n - u_N^{n-1}\|}{\|u_N^{n-1}\|}, \frac{\|v_N^n - v_N^{n-1}\|}{\|v_N^{n-1}\|}\right\}$.

2): **if** $e_n = 0$

Set the time step $\tau_n = \tau_{max}$.

Compute u_N^{n+1}, v_N^{n+1}, φ_N^{n+1}, and r_N^{n+1} by (37)-(40).

3): **elseif** $\sigma|\log_l(e_n)| < 1$

Recalculate the time step $\tau_{n-1} = \max\left\{\tau_{min}, \min\left\{\frac{1}{2}A(e_n, \tau_{n-1}), \tau_{max}\right\}\right\}$.

Recalculate u_N^n, v_N^n, φ_N^n, and r_N^n by (37)-(40).

goto **1)**.

4): **else**

Update the time step $\tau_n = \max\{\tau_{min}, \min\{A(e_n, \tau_{n-1}), \tau_{max}\}$.

Compute u_N^{n+1}, v_N^{n+1}, φ_N^{n+1}, and r_N^{n+1} by (37)-(40).

5): **endif**

3.3. Nonlocal energy conservation laws for schemes (33)-(36) and (37)-(50)

We first investigate the nonlocal energy conservation law of semi-discrete scheme (33)-(36). Taking $\chi_{1N} = \frac{\partial u_N}{\partial t}$ in (33) and adding with its conjugate, taking $\chi_{2N} = \frac{\partial \varphi_N}{\partial t}$ in (34) and $\chi_{3N} = \frac{\partial v_N}{\partial t}$ in (35), combining them with (36), we conclude that the semi-discrete scheme (33)-(36) satisfies the following nonlocal energy conservation law

$$\frac{\mathrm{d}\widetilde{\mathcal{E}}[u_N, v_N, \varphi_N, r_N]}{\mathrm{d}t} = 0, \tag{53}$$

where

$$\widetilde{\mathcal{E}}[u_N, v_N, \varphi_N, r_N] = \frac{1}{2}\left[\kappa_1\|(-\Delta)^{\frac{\alpha}{2}}u_N\|^2 + \kappa_2\|(-\Delta)^{\frac{\beta}{2}}v_N\|^2 + \|\varphi_N\|^2 + \mu^2\|v_N\|^2\right] + \ln(r_N).$$

Now, we move on to discussing the nonlocal energy conservation law of fully discrete scheme (37)-(50). Taking $\chi_{1N} = u_N^{1,0} - u_N^0$ in (42) and adding with its conjugate, we obtain

$$\begin{aligned} &-\frac{\kappa_1}{2}\left(\|(-\Delta)^{\frac{\alpha}{2}}u_N^{1,0}\|^2 - \|(-\Delta)^{\frac{\alpha}{2}}u_N^0\|^2\right) + \frac{\gamma r_N^0}{\exp\left(\mathcal{E}_1[u_N^0, v_N^0]\right)}\left(u_N^0 v_N^0, \overline{u_N^{1,0}} - \overline{u_N^0}\right) \\ &\quad + \frac{\gamma r_N^0}{\exp\left(\mathcal{E}_1[u_N^0, v_N^0]\right)}\left(\overline{u_N^0}v_N^0, u_N^{1,0} - u_N^0\right) = 0. \end{aligned} \tag{54}$$

Then taking $\chi_{2N} = \varphi_N^{1,0} - \varphi_N^0$ in (43), we have

$$\left(\frac{v_N^{1,0} - v_N^0}{\tau_0}, \varphi_N^{1,0} - \varphi_N^0\right) = \frac{1}{2}\left(\|\varphi_N^{1,0}\|^2 - \|\varphi_N^0\|^2\right). \tag{55}$$

If we set $\chi_{3N} = v_N^{1,0} - v_N^0$ in (44), we obtain

$$\begin{aligned} &\left(\frac{\varphi_N^{1,0} - \varphi_N^0}{\tau_0}, v_N^{1,0} - v_N^0\right) + \frac{\kappa_2}{2}\left(\|(-\Delta)^{\frac{\beta}{2}}v_N^{1,0}\|^2 - \|(-\Delta)^{\frac{\beta}{2}}v_N^0\|^2\right) + \frac{\mu^2}{2}\left(\|v_N^{1,0}\|^2 - \|v_N^0\|^2\right) \\ &\quad - \frac{\gamma r_N^0}{\exp\left(\mathcal{E}_1[u_N^0, v_N^0]\right)}\left(|u_N^0|^2, v_N^{1,0} - v_N^0\right) = 0. \end{aligned} \tag{56}$$

Combining (54)-(56) with (45), we have

$$\widetilde{\mathcal{E}}[u_N^{1,0}, v_N^{1,0}, \varphi_N^{1,0}, r_N^{1,0}] = \widetilde{\mathcal{E}}[u_N^0, v_N^0, \varphi_N^0, r_N^0]. \tag{57}$$

Similarly, taking $\chi_{1N} = u_N^1 - u_N^0$ in (47) and adding with its conjugate, taking $\chi_{2N} = \varphi_N^1 - \varphi_N^0$ and $\chi_{3N} = v_N^1 - v_N^0$ in (48) and (49), respectively, and combining with (50), we obtain

$$\widetilde{\mathcal{E}}[u_N^1, v_N^1, \varphi_N^1, r_N^1] = \widetilde{\mathcal{E}}[u_N^0, v_N^0, \varphi_N^0, r_N^0]. \tag{58}$$

By the similar procedure, we obtain the following relation

$$\widetilde{\mathcal{E}}[u_N^{n+1}, v_N^{n+1}, \varphi_N^{n+1}, r_N^{n+1}] = \widetilde{\mathcal{E}}[u_N^n, v_N^n, \varphi_N^n, r_N^n], \quad n = 1, 2, \cdots, \tag{59}$$

where we have taken $\chi_{1N} = u_N^{n+1} - u_N^n$ in (37) and added with its conjugate, taken $\chi_{2N} = \varphi_N^{n+1} - \varphi_N^n$ and $\chi_{3N} = v_N^{n+1} - v_N^n$ in (38) and (39), respectively, and combined them with (40).

Thanks to (57)-(59), we finally obtain the following nonlocal energy conservation law of fully discrete scheme (37)-(50)

$$\widetilde{\mathcal{E}}[u_N^{n+1}, v_N^{n+1}, \varphi_N^{n+1}, r_N^{n+1}] = \cdots = \widetilde{\mathcal{E}}[u_N^1, v_N^1, \varphi_N^1, r_N^1] = \widetilde{\mathcal{E}}[u_N^0, v_N^0, \varphi_N^0, r_N^0], \quad n = 1, 2, \cdots, \tag{60}$$

where

$$\widetilde{\mathcal{E}}[u_N^k, v_N^k, \varphi_N^k, r_N^k] = \frac{1}{2}\left[\kappa_1 \|(-\Delta)^{\frac{\alpha}{2}} u_N^k\|^2 + \kappa_2 \|(-\Delta)^{\frac{\beta}{2}} v_N^k\|^2 + \|\varphi_N^k\|^2 + \mu^2 \|v_N^k\|^2\right] + \ln(r_N^k), \quad k = 0, 1, 2, \cdots. \tag{61}$$

Remark 1. The energy in the continuous sense, denoted by $\widetilde{\mathcal{E}}[u, v, \varphi, r]$, is defined in (31), while the energy in the discrete sense $\widetilde{\mathcal{E}}[u_N^k, v_N^k, \varphi_N^k, r_N^k]$ $(k = 0, 1, 2, \cdots)$ is defined in (61). From these two equations, we can see the definition of the energy in the discrete sense is the same as that in the continuous sense. In other words, these two kinds of definitions can be written as the following unified form:

$$\widetilde{\mathcal{E}}[\Lambda_1, \Lambda_2, \Lambda_3, \Lambda_4] = \frac{1}{2}\left[\kappa_1 \|(-\Delta)^{\frac{\alpha}{2}} \Lambda_1\|^2 + \kappa_2 \|(-\Delta)^{\frac{\beta}{2}} \Lambda_2\|^2 + \|\Lambda_3\|^2 + \mu^2 \|\Lambda_2\|^2\right] + \ln(\Lambda_4).$$

When setting $\Lambda_1 = u$, $\Lambda_2 = v$, $\Lambda_3 = \varphi$, $\Lambda_4 = r$ (resp. $\Lambda_1 = u_N^k$, $\Lambda_2 = v_N^k$, $\Lambda_3 = \varphi_N^k$, $\Lambda_4 = r_N^k$), we obtain the energy in the continuous (resp. discrete) sense. In the practical computations, however, the value of energy in the discrete sense is not equal to that in the continuous sense because of the spatial and temporal discretizations. Numerical examples presented in Fig. 5 in Sec. 4 show that the orders of the relative errors between these two kinds of energies can be $O(10^{-14})$.

3.4. Implements of the ESAV-Hermite-Galerkin scheme

Now, we give the description of the implementation of the fully discrete ESAV-Hermite-Galerkin scheme (37)-(40) with the initialized steps (42)-(50).

For $s = 1, 2, \cdots, d$ and $k, l = 0, 1, \cdots, N$, we introduce the following matrices $\mathbf{P}^{x_s}$, $\mathbf{Q}^{x_s}$, and $\mathbf{R}^{x_s}$ with $(N+1) \times (N+1)$-elements

$$\begin{aligned}
\left(\mathbf{P}^{x_s}\right)_{kl} &= p_{kl}^{x_s} = \left(\widetilde{H}_l(x_s; \lambda_s), \ \widetilde{H}_k(x_s; \lambda_s)\right), \\
\left(\mathbf{Q}^{x_s}\right)_{kl} &= q_{kl}^{x_s} = \left((-\Delta)^{\frac{\alpha}{2}} \widetilde{H}_l(x_s; \lambda_s), \ (-\Delta)^{\frac{\alpha}{2}} \widetilde{H}_k(x_s; \lambda_s)\right), \\
\left(\mathbf{R}^{x_s}\right)_{kl} &= r_{kl}^{x_s} = \left((-\Delta)^{\frac{\beta}{2}} \widetilde{H}_l(x_s; \lambda_s), \ (-\Delta)^{\frac{\beta}{2}} \widetilde{H}_k(x_s; \lambda_s)\right).
\end{aligned}$$

In view of the orthogonality of the Hermite functions in (10), the elements of matrix $\mathbf{P}^{x_s}$ are

$$p_{kl}^{x_s} = \begin{cases} 1, & k = l, \\ 0, & \text{otherwise}. \end{cases}$$

Clearly, the matrix $\mathbf{P}^{x_s}$ is the identity matrix $\mathbf{I}$.

Then, we focus on the computation of the matrices $\mathbf{Q}^{x_s}$ and $\mathbf{R}^{x_s}$. By virtue of the definition of fractional Laplacian (6), the Fourier transform of Hermite functions (11), and the Plancherel formula of the Fourier transform (14), the elements of matrix $\mathbf{Q}^{x_s}$ can be calculated as

$$\begin{aligned}
q_{kl}^{x_s} &= \left((-\Delta)^{\frac{\alpha}{2}} \widetilde{H}_l(x_s; \lambda_s), (-\Delta)^{\frac{\alpha}{2}} \widetilde{H}_k(x_s; \lambda_s)\right) \\
&= \int_{\mathbb{R}} (-\Delta)^{\frac{\alpha}{2}} \widetilde{H}_l(x_s; \lambda_s) \overline{(-\Delta)^{\frac{\alpha}{2}} \widetilde{H}_k(x_s; \lambda_s)} \mathrm{d}x_s \\
&= \int_{\mathbb{R}} \widehat{(-\Delta)^{\frac{\alpha}{2}} \widetilde{H}_l(x_s; \lambda_s)} \, \overline{\widehat{(-\Delta)^{\frac{\alpha}{2}} \widetilde{H}_k(x_s; \lambda_s)}} \mathrm{d}\xi_s \\
&= \int_{\mathbb{R}} |\xi_s|_2^{2\alpha} \, \widehat{\widetilde{H}_l(x_s; \lambda_s)} \, \overline{\widehat{\widetilde{H}_k(x_s; \lambda_s)}} \mathrm{d}\xi_s
\end{aligned} \tag{62}$$

$$= (-i)^l i^k \int_{\mathbb{R}} |\xi_s|_2^{2\alpha} \widetilde{H}_l\left(\xi_s; \frac{1}{\lambda_s}\right) \widetilde{H}_k\left(\xi_s; \frac{1}{\lambda_s}\right) \mathrm{d}\xi_s$$

$$= \frac{(-i)^l i^k}{\lambda_s} \int_{\mathbb{R}} |\xi_s|_2^{2\alpha} \exp\left(-\frac{\xi_s^2}{\lambda_s^2}\right) H_l\left(\frac{\xi_s}{\lambda_s}\right) H_k\left(\frac{\xi_s}{\lambda_s}\right) \mathrm{d}\xi_s, \quad i^2 = -1.$$

Clearly, we need to compute the integral

$$I(k, l, \alpha, \lambda_s) = \int_{\mathbb{R}} |\xi_s|_2^{2\alpha} \exp\left(-\frac{\xi_s^2}{\lambda_s^2}\right) H_l\left(\frac{\xi_s}{\lambda_s}\right) H_k\left(\frac{\xi_s}{\lambda_s}\right) \mathrm{d}\xi_s. \tag{63}$$

Here we employ the Hermite-Gauss quadrature rule associated with generalized Hermite polynomials (13) to compute the above integral, which reads

$$I(k, l, \alpha, \lambda_s) \approx \sum_{j_s=0}^{M} \eta_{j_s} H_l\left(\frac{\xi_{j_s}}{\lambda_s}\right) H_k\left(\frac{\xi_{j_s}}{\lambda_s}\right). \tag{64}$$

In (64), $\{\xi_{j_s}, \eta_{j_s}\}_{j_s=0}^{M}$ are the Hermite-Gauss nodes and the corresponding weights of the generalized Hermite polynomials (13) with respect to the weight function $|\xi_s|_2^{2\alpha} \exp\left(-\frac{\xi_s^2}{\lambda_s^2}\right)$. Note that the numerical integration (64) is exact for all $0 \le k, l \le N$ when $M \ge N$. Because the computation of the matrix $\mathbf{R}^{x_s}$ is the same as that of the matrix $\mathbf{Q}^{x_s}$, we omit the details here for simplicity.

We denote

$$\begin{cases} u_N^n = \displaystyle\sum_{m_1,\cdots,m_d=0}^{N} \widetilde{u}_{m_1\cdots m_d}^n \widetilde{H}_{m_1}(x_1;\lambda_1)\cdots\widetilde{H}_{m_d}(x_d;\lambda_d), \quad v_N^n = \sum_{m_1,\cdots,m_d=0}^{N} \widetilde{v}_{m_1\cdots m_d}^n \widetilde{H}_{m_1}(x_1;\lambda_1)\cdots\widetilde{H}_{m_d}(x_d;\lambda_d), \\ \varphi_N^n = \displaystyle\sum_{m_1,\cdots,m_d=0}^{N} \widetilde{\varphi}_{m_1\cdots m_d}^n \widetilde{H}_{m_1}(x_1;\lambda_1)\cdots\widetilde{H}_{m_d}(x_d;\lambda_d), \quad f_{m_1\cdots m_d}^{n+\frac{1}{2}} = \left(\widetilde{u}_N^{n+\frac{1}{2}}\widetilde{v}_N^{n+\frac{1}{2}}, \widetilde{H}_{m_1}(x_1;\lambda_1)\cdots\widetilde{H}_{m_d}(x_d;\lambda_d)\right), \\ g_{m_1\cdots m_d}^{n+\frac{1}{2}} = \left(|\widetilde{u}_N^{n+\frac{1}{2}}|^2, \widetilde{H}_{m_1}(x_1;\lambda_1)\cdots\widetilde{H}_{m_d}(x_d;\lambda_d)\right). \end{cases} \tag{65}$$

I: One dimensional case. Inserting u_N^n, v_N^n, and φ_N^n expressed in (65) with $d = 1$ into (37)-(39) and setting $\chi_{lN} = \widetilde{H}_{k_1}(x_1;\lambda_1)(l = 1, 2, 3, k_1 = 0, 1, \cdots, N)$, we obtain

$$\begin{cases} i\mathbf{U}^{n+1} - \dfrac{\kappa_1\tau_n}{4}\mathbf{Q}^{x_1}\mathbf{U}^{n+1} = i\mathbf{U}^n + \dfrac{\kappa_1\tau_n}{4}\mathbf{Q}^{x_1}\mathbf{U}^n - \tau_n\widetilde{\rho}^{n+\frac{1}{2}}\mathbf{F}^{n+\frac{1}{2}}, \\ \mathbf{V}^{n+1} - \dfrac{\tau_n}{2}\mathbf{\Phi}^{n+1} = \mathbf{V}^n + \dfrac{\tau_n}{2}\mathbf{\Phi}^n, \\ \mathbf{\Phi}^{n+1} + \dfrac{\kappa_2\tau_n}{2}\mathbf{R}^{x_1}\mathbf{V}^{n+1} + \dfrac{\mu^2\tau_n}{2}\mathbf{V}^{n+1} = \mathbf{\Phi}^n - \dfrac{\kappa_2\tau_n}{2}\mathbf{R}^{x_1}\mathbf{V}^n - \dfrac{\mu^2\tau_n}{2}\mathbf{V}^n + \tau_n\widetilde{\rho}^{n+\frac{1}{2}}\mathbf{G}^{n+\frac{1}{2}}, \end{cases} \tag{66}$$

where

$$\mathbf{U}^{n+1} = \left(\widetilde{u}_1^{n+1}, \widetilde{u}_2^{n+1}, \cdots, \widetilde{u}_N^{n+1}\right)^{\mathrm{T}}, \quad \mathbf{V}^{n+1} = \left(\widetilde{v}_1^{n+1}, \widetilde{v}_2^{n+1}, \cdots, \widetilde{v}_N^{n+1}\right)^{\mathrm{T}}, \quad \mathbf{\Phi}^{n+1} = \left(\widetilde{\varphi}_1^{n+1}, \widetilde{\varphi}_2^{n+1}, \cdots, \widetilde{\varphi}_N^{n+1}\right)^{\mathrm{T}},$$

$$\mathbf{F}^{n+\frac{1}{2}} = \left(f_1^{n+\frac{1}{2}}, f_2^{n+\frac{1}{2}}, \cdots, f_N^{n+\frac{1}{2}}\right)^{\mathrm{T}}, \quad \mathbf{G}^{n+\frac{1}{2}} = \left(g_1^{n+\frac{1}{2}}, g_2^{n+\frac{1}{2}}, \cdots, g_N^{n+\frac{1}{2}}\right)^{\mathrm{T}}.$$

After computing u_N^{n+1}, v_N^{n+1}, and φ_N^{n+1}, we can update r_N^{n+1} by (41) in one-dimensional case.

II: Multidimensional case. When $d = 2$ and $d = 3$, we insert u_N^n, v_N^n, and φ_N^n expressed in (65) into (37)-(39) and take $\chi_{lN} = \widetilde{H}_{k_1}(x_1;\lambda_1)\cdots\widetilde{H}_{k_d}(x_d;\lambda_d)$ for $k_1, \ldots, k_d = 0, 1, \cdots, N$, $l = 1, 2$, and 3. Then, we rewrite (37)-(39) as

$$
\begin{cases}
\displaystyle\sum_{m_1,\cdots,m_d=0}^{N}\left\{i\left(\widetilde{H}_{m_1}\cdots\widetilde{H}_{m_d},\widetilde{H}_{k_1}\cdots\widetilde{H}_{k_d}\right)\widetilde{u}^{n+1}_{m_1\cdots m_d}-\frac{\kappa_1\tau_n}{4}\left(|\boldsymbol{\xi}|_2^{2\alpha}\widehat{\widetilde{H}_{m_1}\cdots\widetilde{H}_{m_d}},\widehat{\widetilde{H}_{k_1}\cdots\widetilde{H}_{k_d}}\right)\widetilde{u}^{n+1}_{m_1\cdots m_d}\right\}=A^n_{1,k_1\cdots k_d},\\
\displaystyle\sum_{m_1,\cdots,m_d=0}^{N}\left\{(\widetilde{H}_{m_1}\cdots\widetilde{H}_{m_d},\widetilde{H}_{k_1}\cdots\widetilde{H}_{k_d})\widetilde{v}^{n+1}_{m_1\cdots m_d}-\frac{\tau_n}{2}\left(\widetilde{H}_{m_1}\cdots\widetilde{H}_{m_d},\widetilde{H}_{k_1}\cdots\widetilde{H}_{k_d}\right)\widetilde{\varphi}^{n+1}_{m_1\cdots m_d}\right\}=A^n_{2,k_1\cdots k_d},\\
\displaystyle\sum_{m_1,\cdots,m_d=0}^{N}\left\{\left(\widetilde{H}_{m_1}\cdots\widetilde{H}_{m_d},\widetilde{H}_{k_1}\cdots\widetilde{H}_{k_d}\right)\widetilde{\varphi}^{n+1}_{m_1\cdots m_d}+\frac{\kappa_2\tau_n}{2}\left(|\boldsymbol{\xi}|_2^{2\beta}\widehat{\widetilde{H}_{m_1}\cdots\widetilde{H}_{m_d}},\widehat{\widetilde{H}_{k_1}\cdots\widetilde{H}_{k_d}}\right)\widetilde{u}^{n+1}_{m_1\cdots m_d}\right.\\
\qquad\left.+\frac{\mu^2\tau_n}{2}\left(\widetilde{H}_{m_1}\cdots\widetilde{H}_{m_d},\widetilde{H}_{k_1}\cdots\widetilde{H}_{k_d}\right)\widetilde{v}^{n+1}_{m_1\cdots m_d}\right\}=A^n_{3,k_1\cdots k_d},
\end{cases}
\tag{67}
$$

where the expressions of $A^n_{1,k_1\cdots k_d}$, $A^n_{2,k_1\cdots k_d}$, and $A^n_{3,k_1\cdots k_d}$ are given as

$$
\begin{aligned}
A^n_{1,k_1\cdots k_d}=&\sum_{m_1,\cdots,m_d=0}^{N}\left\{i\left(\widetilde{H}_{m_1}\cdots\widetilde{H}_{m_d},\widetilde{H}_{k_1}\cdots\widetilde{H}_{k_d}\right)\widetilde{u}^{n}_{m_1\cdots m_d}+\frac{\kappa_1\tau_n}{4}\left(|\boldsymbol{\xi}|_2^{2\alpha}\widehat{\widetilde{H}_{m_1}\cdots\widetilde{H}_{m_d}},\widehat{\widetilde{H}_{k_1}\cdots\widetilde{H}_{k_d}}\right)\widetilde{u}^{n}_{m_1\cdots m_d}\right\}\\
&-\tau_n\widetilde{\rho}^{n+\frac{1}{2}}f^{n+\frac{1}{2}}_{k_1\cdots k_d},\\
A^n_{2,k_1\cdots k_d}=&\sum_{m_1,\cdots,m_d=0}^{N}\left\{(\widetilde{H}_{m_1}\cdots\widetilde{H}_{m_d},\widetilde{H}_{k_1}\cdots\widetilde{H}_{k_d})\widetilde{v}^{n}_{m_1\cdots m_d}+\frac{\tau_n}{2}\left(\widetilde{H}_{m_1}\cdots\widetilde{H}_{m_d},\widetilde{H}_{k_1}\cdots\widetilde{H}_{k_d}\right)\widetilde{\varphi}^{n}_{m_1\cdots m_d}\right\},\\
A^n_{3,k_1\cdots k_d}=&\sum_{m_1,\cdots,m_d=0}^{N}\left\{\left(\widetilde{H}_{m_1}\cdots\widetilde{H}_{m_d},\widetilde{H}_{k_1}\cdots\widetilde{H}_{k_d}\right)\widetilde{\varphi}^{n}_{m_1\cdots m_d}-\frac{\kappa_2\tau_n}{2}\left(|\boldsymbol{\xi}|_2^{2\beta}\widehat{\widetilde{H}_{m_1}\cdots\widetilde{H}_{m_d}},\widehat{\widetilde{H}_{k_1}\cdots\widetilde{H}_{k_d}}\right)\widetilde{u}^{n}_{m_1\cdots m_d}\right.\\
&\left.-\frac{\mu^2\tau_n}{2}\left(\widetilde{H}_{m_1}\cdots\widetilde{H}_{m_d},\widetilde{H}_{k_1}\cdots\widetilde{H}_{k_d}\right)\widetilde{v}^{n}_{m_1\cdots m_d}\right\}+\tau_n\widetilde{\rho}^{n+\frac{1}{2}}g^{n+\frac{1}{2}}_{k_1\cdots k_d}.
\end{aligned}
$$

Because the terms $|\boldsymbol{\xi}|_2^{2\alpha}=(\xi_1^2+\cdots+\xi_d^2)^{\alpha}$ and $|\boldsymbol{\xi}|_2^{2\beta}=(\xi_1^2+\cdots+\xi_d^2)^{\beta}$ in (67) are the nonseparable variable coefficients, it is very expensive to calculate the stiffness matrix explicitly and to solve the resulting algebraic system by the direct method. Hence, we shall use the iterative approach with the suitable separable problem as the preconditioner system. Here, the preconditioner systems are constructed as

$$
\begin{cases}
\displaystyle\sum_{m_1,\cdots,m_d=0}^{N}\left\{i\left(\widetilde{H}_{m_1}\cdots\widetilde{H}_{m_d},\widetilde{H}_{k_1}\cdots\widetilde{H}_{k_d}\right)\widetilde{u}^{*,n+1}_{m_1\cdots m_d}-\frac{\kappa_1\tau_n}{4}\left(\sum_{l=1}^{d}|\xi_l|_2^{2\alpha}\widehat{\widetilde{H}_{m_1}\cdots\widetilde{H}_{m_d}},\widehat{\widetilde{H}_{k_1}\cdots\widetilde{H}_{k_d}}\right)\widetilde{u}^{*,n+1}_{1,m_1\cdots m_d}\right\}\\
\qquad=A^n_{1,k_1\cdots k_d},\\
\displaystyle\sum_{m_1,\cdots,m_d=0}^{N}\left\{(\widetilde{H}_{m_1}\cdots\widetilde{H}_{m_d},\widetilde{H}_{k_1}\cdots\widetilde{H}_{k_d})\widetilde{v}^{*,n+1}_{m_1\cdots m_d}-\frac{\tau_n}{2}\left(\widetilde{H}_{m_1}\cdots\widetilde{H}_{m_d},\widetilde{H}_{k_1}\cdots\widetilde{H}_{k_d}\right)\widetilde{\varphi}^{*,n+1}_{m_1\cdots m_d}\right\}=A^n_{2,k_1\cdots k_d},\\
\displaystyle\sum_{m_1,\cdots,m_d=0}^{N}\left\{\left(\widetilde{H}_{m_1}\cdots\widetilde{H}_{m_d},\widetilde{H}_{k_1}\cdots\widetilde{H}_{k_d}\right)\widetilde{\varphi}^{*,n+1}_{m_1\cdots m_d}+\frac{\kappa_2\tau_n}{2}\left(\sum_{l=1}^{d}|\xi_l|_2^{2\beta}\widehat{\widetilde{H}_{m_1}\cdots\widetilde{H}_{m_d}},\widehat{\widetilde{H}_{k_1}\cdots\widetilde{H}_{k_d}}\right)\widetilde{u}^{*,n+1}_{m_1\cdots m_d}\right.\\
\qquad\left.+\frac{\mu^2\tau_n}{2}\left(\widetilde{H}_{m_1}\cdots\widetilde{H}_{m_d},\widetilde{H}_{k_1}\cdots\widetilde{H}_{k_d}\right)\widetilde{v}^{*,n+1}_{m_1\cdots m_d}\right\}=A^n_{3,k_1\cdots k_d}.
\end{cases}
\tag{68}
$$

In the above preconditioner system, the variable coefficients are of the separable forms, i.e., $\sum_{l=1}^{d}|\xi_l|_2^{2\alpha}$ and $\sum_{l=1}^{d}|\xi_l|_2^{2\beta}$, which indicates we can easily compute the stiffness matrix and efficiently solve the resulting algebraic system by the matrix decomposition method [35] with the help of the following generalized eigenvalue problems:

$$
\mathbf{P}^{x_s}\mathbf{w}_1^{x_s}=\omega_1^{x_s}\mathbf{Q}^{x_s}\mathbf{w}_1^{x_s},\quad \mathbf{P}^{x_s}\mathbf{w}_2^{x_s}=\omega_2^{x_s}\mathbf{R}^{x_s}\mathbf{w}_2^{x_s},\ s=1,2,\ldots,d.
\tag{69}
$$

From Fig. 1, we observe that all the eigenvalues of matrices $\mathbf{Q}^{x_s}$ and $\mathbf{R}^{x_s}$ are real and positive. We can efficiently solve the linear system (67) by iterative methods including the preconditioned conjugate gradient method [34], GMRES method [37],

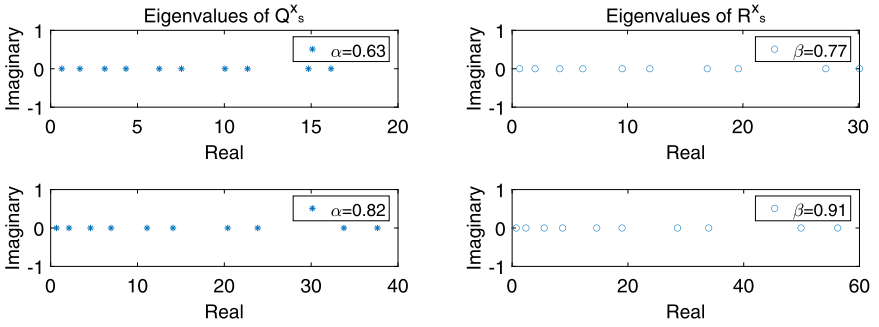

Fig. 1. Distributions of eigenvalues for matrices $\mathbf{Q}^{x_s}$ (plot(a)) and $\mathbf{R}^{x_s}$ (plot (b)) with different values of α and β.

and Picard iterative method [39]. The preconditioner system (68) in two dimensional case can be rewritten as the following matrix form:

$$\begin{cases} i\mathbf{U}^{*,n+1} - \dfrac{\kappa_1\tau_n}{4}\left(\mathbf{Q}^{x_1}\mathbf{U}^{*,n+1} + \mathbf{U}^{*,n+1}\mathbf{Q}^{x_2}\right) = \mathbf{A}_1^n, \\ \mathbf{V}^{*,n+1} - \dfrac{\tau_n}{2}\mathbf{\Phi}^{*,n+1} = \mathbf{A}_2^n, \\ \mathbf{\Phi}^{*,n+1} + \dfrac{\kappa_2\tau_n}{2}(\mathbf{R}^{x_1}\mathbf{V}^{*,n+1} + \mathbf{V}^{*,n+1}\mathbf{R}^{x_2}) + \dfrac{\mu^2\tau_n}{2}\mathbf{V}^{*,n+1} = \mathbf{A}_3^n, \end{cases}$$

where

$$\mathbf{U}^{*,n+1} = \left(\widetilde{u}_{lm}^{*,n+1}\right)_{l,m=0}^{N}, \quad \mathbf{V}^{*,n+1} = \left(\widetilde{v}_{lm}^{*,n+1}\right)_{l,m=0}^{N}, \quad \mathbf{\Phi}^{*,n+1} = \left(\widetilde{\varphi}_{lm}^{*,n+1}\right)_{l,m=0}^{N}, \quad \mathbf{A}_k^n = \left(A_{k,lm}^n\right)_{l,m=0}^{N}, \quad k = 1,2,3.$$

After calculating the values of u_N^{n+1}, v_N^{n+1}, and φ_N^{n+1}, we can update r_N^{n+1} by (41) in two- and three-dimensional cases.

By the similar procedures, we can calculate the values of $u_N^{1,0}$ (resp. u_N^1), $v_N^{1,0}$ (resp. v_N^1), $\varphi_N^{1,0}$ (resp. φ_N^1), and $r^{1,0}$ (resp. r_N^1) from (42)-(46) (resp. (47)-(50)). For simplicity, we omit the descriptions here.

Remark 2. In the practical computations, we notice that the variable $r(t)$ which is defined by $r(t) = \exp(\mathcal{E}_1[u,v]) = \exp\left(-\gamma\int_{\mathbb{R}^d}|u|^2 v d\mathbf{x}\right)$ may tend to zero if $\mathcal{E}_1[u,v] \ll 0$. To avoid the singularity, we can add a sufficiently large positive constant C into $r(t)$. In particular, we define a new exponential scalar auxiliary variable $\Upsilon(t)$:

$$\Upsilon(t) = \exp\left(\frac{\mathcal{E}_1[u,v]}{C}\right) = \exp\left(-\frac{\gamma}{C}\int_{\mathbb{R}^d}|u|^2 v d\mathbf{x}\right).$$

Because C is a sufficiently large positive constant, we conclude that the new variable $\Upsilon(t)$ is bounded from below. Therefore, this improvement can avoid the singularity. By introducing the new variable $\Upsilon(t)$, we transform the system (26)-(29) as

$$\begin{cases} i\dfrac{\partial u}{\partial t} - \dfrac{\kappa_1}{2}(-\Delta)^\alpha u + \dfrac{\gamma\Upsilon}{\exp\left(\frac{\mathcal{E}_1}{C}\right)}(uv) = 0, & \text{in } \mathbb{R}^d\times(0,T], \quad (70) \\ \dfrac{\partial v}{\partial t} = \varphi, & \text{in } \mathbb{R}^d\times(0,T], \quad (71) \\ \dfrac{\partial \varphi}{\partial t} + \kappa_2(-\Delta)^\beta v + \mu^2 v - \dfrac{\gamma\Upsilon}{\exp\left(\frac{\mathcal{E}_1}{C}\right)}(|u|^2) = 0, & \text{in } \mathbb{R}^d\times(0,T], \quad (72) \end{cases}$$

where $\Upsilon(t)$ satisfies the following ODE

$$\frac{\mathrm{d}\ln(\Upsilon(t))}{\mathrm{d}t} = -\frac{\gamma\Upsilon}{C\exp\left(\frac{\mathcal{E}_1}{C}\right)}\int_{\mathbb{R}^d}\left[|u|^2\frac{\partial v}{\partial t} + \overline{u}v\frac{\partial u}{\partial t} + uv\frac{\partial \overline{u}}{\partial t}\right]\mathrm{d}\mathbf{x}. \quad (73)$$

Now, we discuss the energy of the above system involving new variable $\Upsilon(t)$. Taking the inner product of (70) with $\frac{\partial u}{\partial t}$ and adding with its conjugate, taking the inner products of (71) and (72) with $\frac{\partial \varphi}{\partial t}$ and $\frac{\partial v}{\partial t}$, respectively, and combining them with (73), we obtain the following nonlocal energy conservation law

$$\frac{\mathrm{d}\widetilde{\mathcal{E}}_{\Upsilon}[u,v,\varphi,\Upsilon]}{\mathrm{d}t}=0, \tag{74}$$

where

$$\widetilde{\mathcal{E}}_{\Upsilon}[u,v,\varphi,\Upsilon]=\frac{1}{2}\left[\kappa_1\|(-\Delta)^{\frac{\alpha}{2}}u\|^2+\kappa_2\|(-\Delta)^{\frac{\beta}{2}}v\|^2+\|\varphi\|^2+\mu^2\|v\|^2\right]+C\ln(\Upsilon). \tag{75}$$

Because $\ln(\Upsilon(t))=\ln\left(\exp\left(\frac{\mathcal{E}_1[u,v]}{C}\right)\right)=\frac{\mathcal{E}_1[u,v]}{C}$ and $\varphi=\frac{\partial v}{\partial t}$, we have $\widetilde{\mathcal{E}}_{\Upsilon}[u,v,\varphi,\Upsilon]=\mathcal{E}[u,v]$. In other words, the energy involving new variable $\Upsilon(t)$ is exactly equal to the original energy defined in (24). In the practical calculation, because the parameters κ_1, κ_2, and μ^2 are positive, we can set the positive constant $C=\frac{1}{2}\Big[\kappa_1\|(-\Delta)^{\frac{\alpha}{2}}u_0\|^2+\kappa_2\|(-\Delta)^{\frac{\beta}{2}}v_0\|^2+\|v_0^{\diamond}\|^2+\mu^2\|v_0\|^2\Big]+|\mathcal{E}_1[u_0,v_0]|$. Here, u_0, v_0, and $v_0^{\diamond}$ are the initial conditions (3). A direct calculation yields $-1\le\frac{\mathcal{E}_1[u,v]}{C}\le 1$, which reveals that the new variable $\Upsilon(t)$ satisfies $e^{-1}\le\Upsilon(t)\le e$. Then we can construct the fully discrete scheme for system (70)-(73) with new variable $\Upsilon(t)$, where the proposed methodology can still be valid.

4. Numerical simulations

In this section, we give a series of numerical tests to show the effectiveness of the linearized, energy-conserving, and time-stepping-varying ESAV-Hermite-Galerkin spectral scheme (37)-(40) with the initialized step (42)-(50) for KGS system (1)-(4). The first example is provided to demonstrate the convergence rate with uniform time-stepping, the efficiency of the time-adaptivity techniques, and the nonlocal energy conservation law of the scheme. In the following, we give the simulations of the interactions of 2D/3D vector solitons. We perform all computations by Matlab R2016b in a 3.70 GHz PC with i9-10900K CPU, 16 GB RAM, and Win 10 operating system.

4.1. Tests of the features of the scheme

For KGS system (1)-(4) in $\mathbb{R}^3$, we take the initial conditions as

$$\begin{cases} u_0=(1+i)\exp(-(5x_1)^2-(5x_2)^2-(5x_3)^2),\ i^2=-1,\\ v_0=v_0^{\diamond}=\exp(-(5x_1)^2-(5x_2)^2-(5x_3)^2). \end{cases}$$

Because the exact solutions of such problem are unknown, we calculate the errors caused by the proposed scheme with uniform time-stepping as follows: For the discretization parameters N and τ, let $u_N^T(N,\tau)$ be the numerical solutions at T. The L^2-error in spatial direction with sufficiently small τ is defined as

$$R(N)=\|u_N^T(\widetilde{N},\tau)-u_N^T(N,\tau)\|,\quad N<\widetilde{N}.$$

Denote by

$$E(\tau)=\|u_N^T(N,\widetilde{\tau})-u_N^T(N,\tau)\|,\quad \tau>\widetilde{\tau},$$

the L^2-error in temporal direction for sufficiently large N. And the L^∞-errors can be defined by a similar way.

Tests of convergence rate with uniform time-stepping. We show the L^2- and L^∞-errors v.s. N for different values of α and β in Fig. 2, where the log-scale is taken for the error-axis. Obviously, the results reveal that the decays of the L^2- and L^∞-errors in the log-scale are linear with respect to N. Thus, the proposed scheme with uniform time-stepping can attain the spectral accuracy in spatial approximation.

In Table 1, we study the convergent properties of the scheme with uniform time-stepping in temporal direction. Clearly, the results show that the temporal convergence orders of L^2- and L^∞-errors are $O(\tau^2)$ for different values of α and β.

Tests of adaptive time-stepping strategies. Now, we investigate the performance of the adaptive time-stepping strategies described in Algorithms 1 and 2. We first check the validity of these two strategies. As comparison, we calculate the reference solutions by a small uniform time step size $\tau=1e-2$. In Fig. 3, we show the isosurfaces of the numerical solutions solved by our proposed scheme with uniform time-stepping and Algorithms 1 and 2. It can be seen from the figure that the adaptive time solutions by Algorithm 1 (resp. Algorithm 2) given in the second (resp. third) column agree with the reference solutions given in the first column very well.

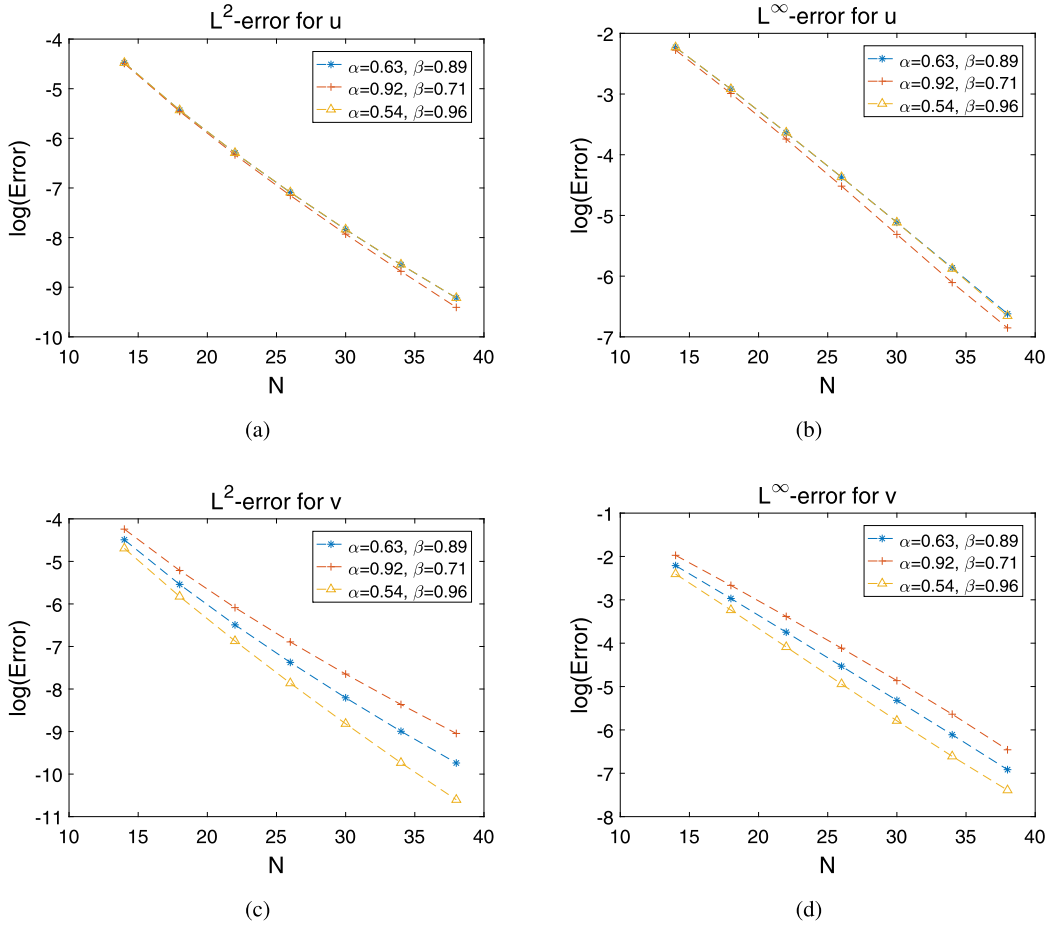

Fig. 2. L^2- and L^∞-errors v.s. N for different values of α and β. The parameters are $\tau = 1e-2$, $T = 1$, $\kappa_1 = \kappa_2 = 0.01$, $\gamma = 0.08$, $\mu = 0.06$, and $\lambda_s = 2.5$ $(s = 1, 2, 3)$. Plot (a): L^2-errors for u; Plot (b): L^∞-errors for u; Plot (c): L^2-errors for v; Plot (d): L^∞-errors for v.

Table 1
L^2- and L^∞-errors and the corresponding convergence orders in the temporal direction. The parameters are $N = 30$, $T = 1$, $\kappa_1 = \kappa_2 = 0.01$, $\gamma = 0.08$, $\mu = 0.06$, and $\lambda_s = 2.5$ $(s = 1, 2, 3)$.

$\alpha = 0.60$, $\beta = 0.80$	Numerical results for u				Numerical results for v			
τ	L^2-Error	Order	L^∞-Error	Order	L^2-Error	Order	L^∞-Error	Order
1/50	5.53438e-8	1.98	2.27266e-6	1.98	6.73917e-8	2.00	2.24638e-6	2.00
1/100	1.40353e-8	1.99	5.76347e-7	1.99	1.68463e-8	2.00	5.61504e-7	2.00
1/200	3.53367e-9	1.99	1.45107e-7	1.99	4.21115e-9	2.00	1.40356e-7	2.00
1/400	8.86516e-10	–	3.64040e-8	–	1.05286e-9	–	3.50917e-8	–
1/800	–	–	–	–	–	–	–	
$\alpha = 0.75$, $\beta = 0.63$	Numerical results for u				Numerical results for v			
τ	L^2-Error	Order	L^∞-Error	Order	L^2-Error	Order	L^∞-Error	Order
1/50	2.52310e-8	1.98	1.02925e-6	1.98	5.19262e-8	2.00	2.07164e-6	2.00
1/100	6.38510e-9	1.99	2.60488e-7	1.99	1.29679e-8	2.00	5.17319e-7	2.00
1/200	1.60593e-9	2.00	6.55181e-8	2.00	3.24004e-9	2.00	1.29247e-7	2.00
1/400	4.02683e-10	–	1.64289e-8	–	8.09931e-10	–	3.23078e-8	–
1/800	–	–	–	–	–	–	–	
$\alpha = 0.83$, $\beta = 0.59$	Numerical results for u				Numerical results for v			
τ	L^2-Error	Order	L^∞-Error	Order	L^2-Error	Order	L^∞-Error	Order
1/50	3.40613e-8	1.99	1.02925e-6	1.98	4.18576e-8	2.01	1.66051e-6	2.01
1/100	8.58562e-9	1.99	2.60488e-7	1.99	1.04239e-8	2.00	4.13350e-7	2.00
1/200	2.15516e-9	2.00	6.55181e-8	2.00	2.60068e-9	2.00	1.03105e-7	2.00
1/400	5.39878e-10	–	1.64289e-8	–	6.49656e-10	–	2.57532e-8	–
1/800	–	–	–	–	–	–	–	

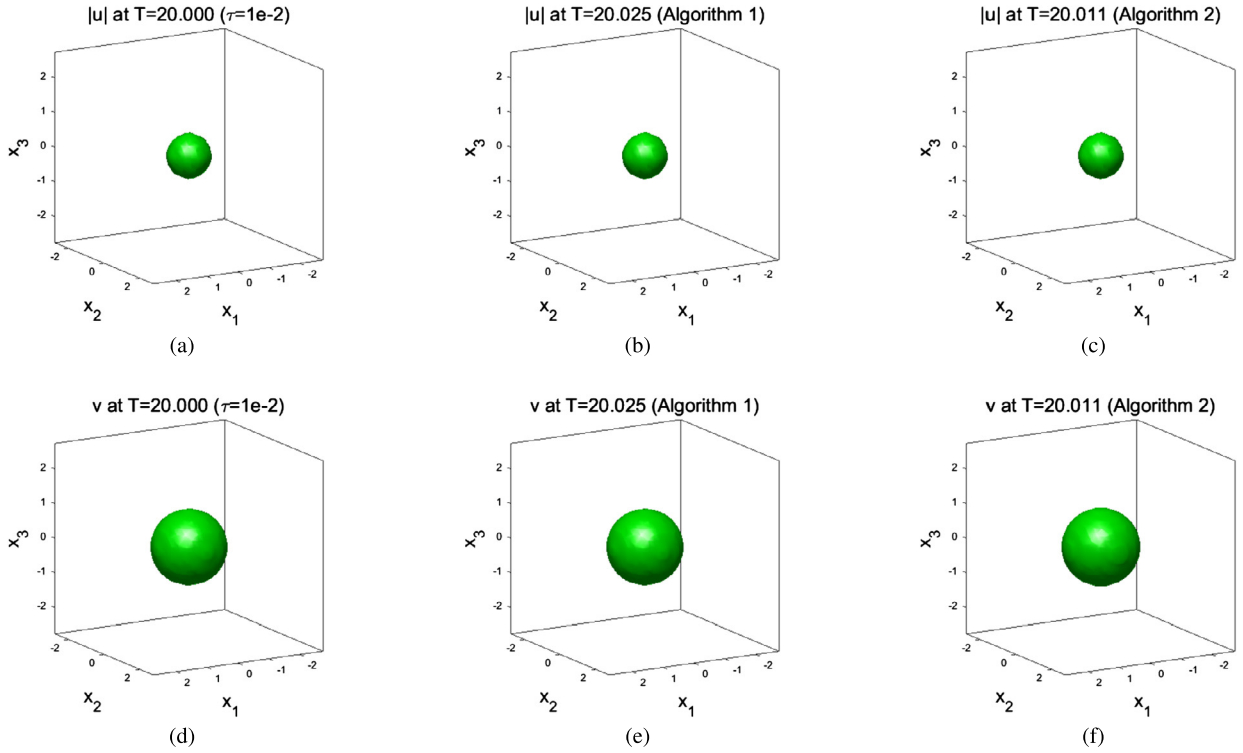

Fig. 3. Isosurfaces $|u| = 0.01$ and $v = -0.03$ of the numerical solutions. The first column: small uniform time-stepping $\tau = 1e-2$. The second column: Algorithm 1. The third column: Algorithm 2. The parameters are $N = 20$, $\alpha = 0.57$, $\beta = 0.80$, $\kappa_1 = \kappa_2 = 0.01$, $\gamma = 0.08$, $\mu = 0.06$, $\tau_{min} = 1e-2$, $\tau_{max} = 1e-1$, and $\lambda_s = 2.5$ $(s = 1, 2, 3)$.

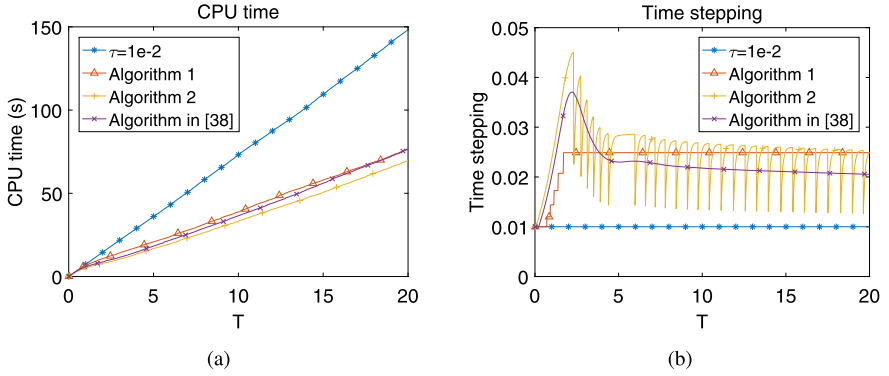

Fig. 4. Numerical comparisons between the uniform time-stepping and adaptive time-stepping (Algorithms 1 and 2 and Algorithm in [38]). Plot (a): Comparison of CPU time. Plot (b): Comparison of time step size. The parameters are the same as that in Fig. 3.

In Ref. [38], the authors proposed the following formula for updating the time-stepping

$$A_{dp}(e, \tau) = \rho \left(\frac{tol}{e} \right)^{1/2} \tau, \tag{76}$$

where $\rho > 0$ is the safety coefficient, tol is a given tolerance, e is defined in (51). In our computing, we set $\rho = 0.9$ and $tol = 1e-2$. Because this adaptive strategy has been successfully applied for solving many problems [25], we shall compare the proposed Algorithms 1 and 2 in this paper with the Algorithm in [38]. To show the efficiency of the adaptive time-stepping strategies, we depict the CPU time of the uniform and adaptive time-stepping strategies in plot (a) in Fig. 4. We can see from the plot that: i) Compared with the uniform time-stepping, Algorithms 1 and 2 and Algorithm in [38] can save about 50% of the CPU time; ii) The CPU times for these three time-stepping strategies are very close to each other. Plot (b) in Fig. 4 shows the variations of the time step size for the Algorithms 1 and 2 and Algorithm in [38]. This plot indicates that

Table 2
Number of iterations for Algorithms 1 and 2 with different values of α and β. The parameters are the same as that in Fig. 3.

	Time level n	Number of iterations for Algorithm 1	Number of iterations for Algorithm 2
$\alpha = 0.57,\ \beta = 0.80$	10	7	7
	50	7	7
	100	7	7
	120	7	7
$\alpha = 0.63,\ \beta = 0.83$	10	8	8
	50	8	8
	100	8	8
	120	8	8
$\alpha = \beta = 0.54$	10	7	7
	50	7	7
	100	7	7
	120	7	7

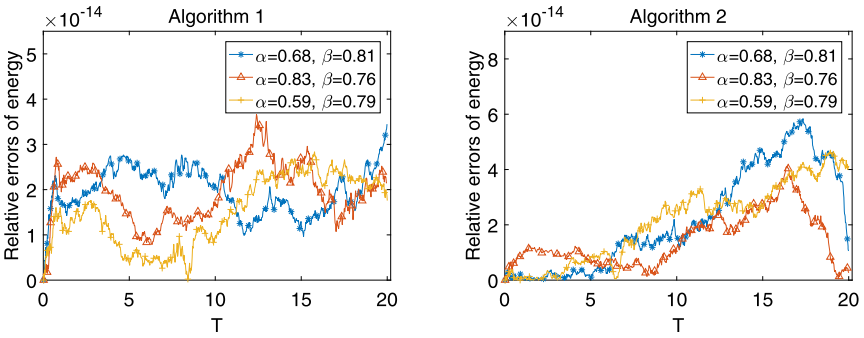

Fig. 5. The relative errors of nonlocal energy for different values of α and β. Plot (a): Algorithm 1. Plot (b): Algorithm 2. The parameters are the same as that in Fig. 3.

the variation of time step size in Algorithms 1 is the step function, while the change of the time step size in Algorithms 2 is oscillating.

We now show the effectiveness of the preconditioned iterative method for Algorithms 1 and 2, where the threshold of the iteration is set as 10^{-10}. We list in Table 2 the iteration numbers of the GMRES method for solving (67) with preconditioner (68) at different time levels n, which indicates the iteration numbers are independent of n.

Tests of nonlocal energy conservation law. We now check the discrete nonlocal energy conservation law of the system solved by the proposed scheme. Plots (a) and (b) in Fig. 5 show the relative errors of the nonlocal energy calculated by Algorithms 1 and 2, respectively. The results demonstrate that both the Algorithms 1 and 2 can preserve the nonlocal energy very well in discrete sense for different values of α and β.

4.2. Interactions of circular vector solitons in $\mathbb{R}^2$

As the applications of the proposed ESAV-Hermite-Galerkin spectral scheme, we study the collisions of circular vector solitons described by KGS system (1)-(4) in two dimensional case with the following initial conditions

$$\begin{cases} u_0 = \dfrac{(1+i)}{10}\displaystyle\sum_{k=0}^{1}\sum_{j=0}^{1} \operatorname{sech}\left(9(x_1-(-1)^k 3)^2 + 9(x_2-(-1)^j 3)^2\right), \ i^2=-1, \\ v_0 = \dfrac{1}{10}\displaystyle\sum_{k=0}^{1}\sum_{j=0}^{1} \exp\left(-5(x_1-(-1)^k 3)^2 - 5(x_2-(-1)^j 3)^2\right), \qquad v_0^{\diamond} = \dfrac{1}{10}\operatorname{sech}(x_1^2+x_2^2). \end{cases} \tag{77}$$

Using the ESAV-Hermite-Galerkin spectral scheme with Algorithm 2, we set $N = 70$, $\kappa_1 = \kappa_2 = 0.5$, $\mu = 0.6$, $\gamma = 0.08$, $\alpha = 0.60$, $\beta = 0.80$, an $\lambda_s = 1.2 (s = 1, 2)$ in our computations.

For a better understanding of the interactions of circular vector solitons in two-dimensional case, the time evolutions of components u and v are presented in Figs. 6 and 7, respectively. Plots (a) and (e) in Fig. 6 respectively show the surface and density plots of u at $t = 0$, which reveals the initial conditions of u is composed by four circular solitons. From plots (b)

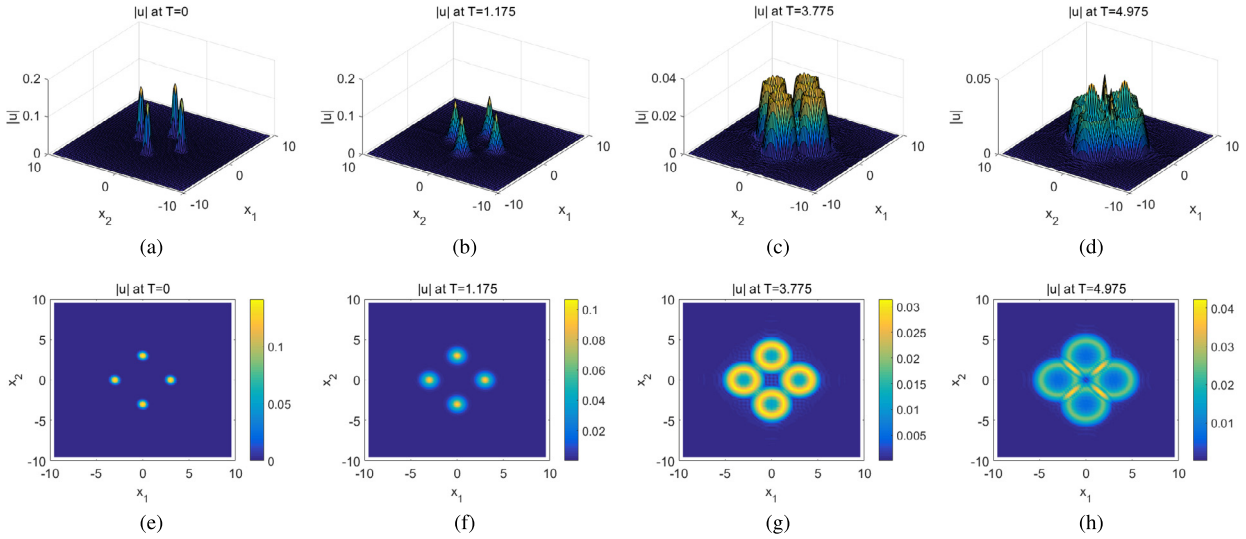

Fig. 6. Interactions of 2D circular vector solitons for component u. The first row: surface plots; The second row: density plots.

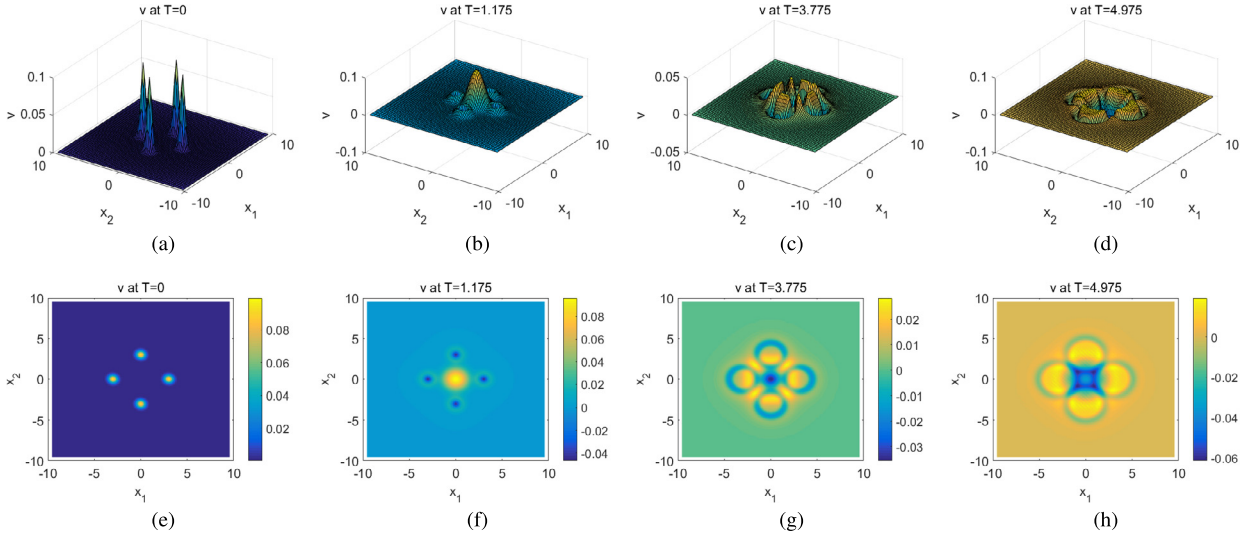

Fig. 7. Interactions of 2D circular vector solitons for component v. The first row: surface plots; The second row: density plots.

and (f), we observe that these four circular solitons radiate. As is shown in plots (c) and (g) in Fig. 6, the circular solitons begin to collide with time going on, and their amplitudes decrease. Plots (d) and (h) depict the interaction of circular vector solitons for u, which shows the values of the contact segments increase because of the collisions. Plots (a) and (e) in Fig. 7 also show the component v consists of four circular solitons at the initial step. However, plots (b) and (f) depict one circular soliton in the center of the region is created while the original four solitons decrease as times goes on. From plots (c) and (g), we can see the central peak decreases while the contact segments of the original four solitons increase. Plots (d) and (h) show that the central peak continues to decrease and radiate as time goes on.

4.3. Interactions of elliptical vector solitons in $\mathbb{R}^3$

In this subsection, we utilize ESAV-Hermite-Galerkin spectral scheme with Algorithm 2 to investigate the collisions of 3D elliptical vector solitons KGS system (1)-(4). The initial conditions are given as

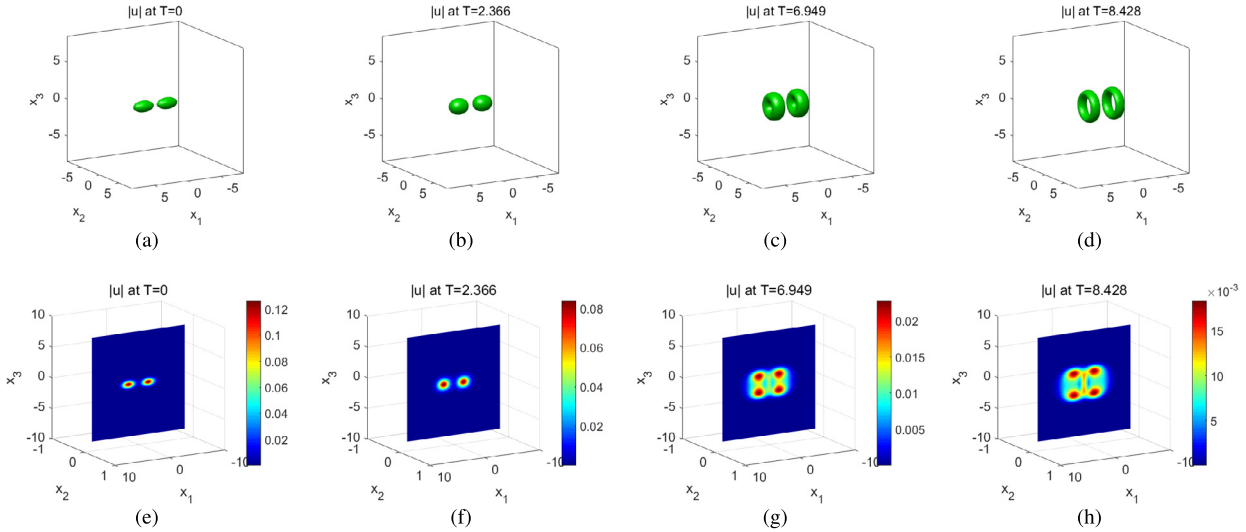

Fig. 8. Interactions of 3D elliptical vector solitons for component u. The first row: isosurfaces $|u| = 0.015$. The second row: slices of u at $x_2 = 0$.

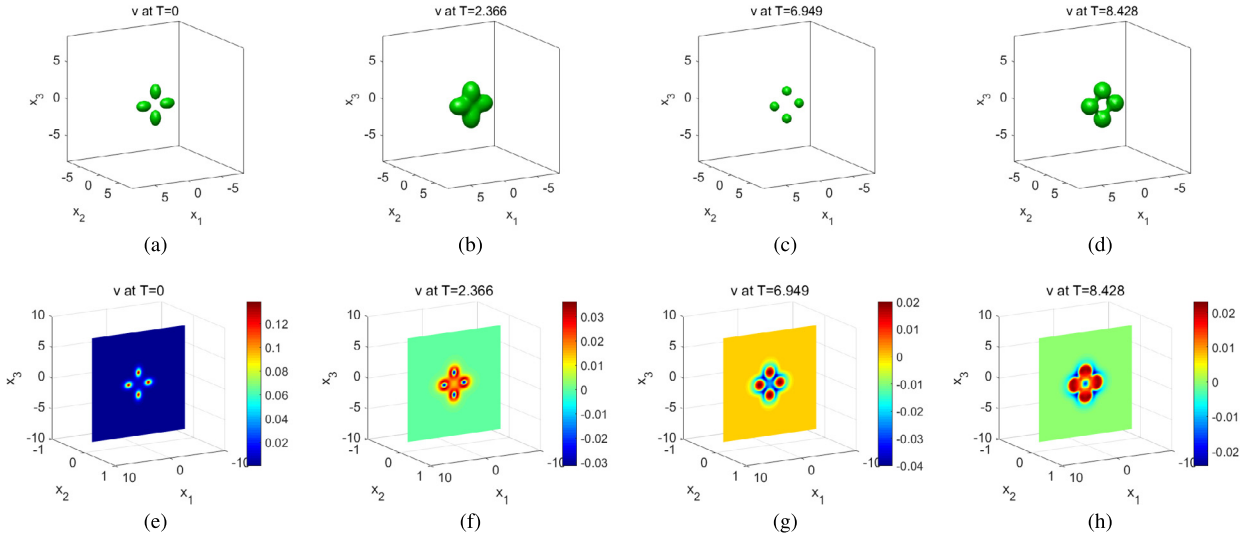

Fig. 9. Interactions of 3D elliptical vector solitons for component v. The first row: isosurfaces $v = 0.01$. The second row: slices of v at $x_2 = 0$.

$$\begin{cases} u_0 = \dfrac{(1+i)}{10}\displaystyle\sum_{k=0}^{1}\exp\left(-(x_1-(-1)^k 1.8)^2-(2x_2)^2-(2x_3)^2\right), \quad i^2=-1, \\ v_0 = \dfrac{1}{10}\displaystyle\sum_{k=0}^{1}\sum_{j=0}^{1}\exp\left(1-\sqrt{\dfrac{(4(x_1-(-1)^k 1.8))^2}{2}+(4x_2)^2+(4(x_3-(-1)^j 1.8)^2}\right), \\ v_0^{\diamond} = \dfrac{1}{10}\displaystyle\sum_{k=0}^{1}\sum_{j=0}^{1}\arctan\left(\exp\left(1-\sqrt{\dfrac{(4(x_1-(-1)^k 1.8))^2}{2}+(4x_2)^2+(4(x_3-(-1)^j 1.8)^2}\right)\right). \end{cases} \tag{78}$$

We set the parameters in the simulations as $\tau_{min} = 1e-2$, $\tau_{max} = 1e-1$, $N = 60$, $\kappa_1 = 0.3$, $\kappa_2 = 0.08$, $\mu = 0.6$, $\gamma = 0.08$, $\alpha = 0.60$, $\beta = 0.80$, an $\lambda_s = 1.2 (s = 1, 2, 3)$.

We study the interactions of elliptical solitons for component u in Fig. 8, where the first and the second rows show the isosurface $|u| = 0.015$ and slices at $x_2 = 0$, respectively. Plot (a) indicates that the isosurfaces $|u| = 0.015$ at $T = 0$ are composed by two separated ellipsoids. As time goes on, we can observe from plot (b) that these two ellipsoids radiate. From plot (c), it can be seen the isosurface $|u| = 0.015$ continues to expand but the surfaces shrink along the x_2-axis. Plot

(d) shows that isosurface $|u| = 0.015$ evolves into two circular rings like doughnuts with time going on. In plots (e)-(h) in Fig. 8, we present the slices of $|u|$ at $x_2 = 0$ to show the time evolutions of component u, which reveals that the interaction processes are complex. Fig. 9 indicates the collisions of elliptical solitons for component v, where the isosurfaces $v = 0.01$ and the slices at $x_2 = 0$ are given in the first and second rows, respectively. From the first row, we can see isosurface $v = 0.01$ consists of four separated ellipsoids at the initial step (plot (a)); then radiations and collisions of the solitons continue to form up to $T = 2.366$ (plot (b)); with time going on, the isosurface $v = 0.01$ shrinks and four separated spheres are created (plot (c)); finally, the isosurface $v = 0.01$ radiates again and the collision occurs for the second time (plot (d)). The time evolutions of slices of v at $x_2 = 0$ are presented in plots (e)-(h) in Fig. 9, which indicates the interactions of elliptical solitons for the component v can form complex structures.

5. Conclusion

When constructing numerical method for nonlocal Klein-Gordon-Schrödinger system (1)-(4) with fractional Laplacian in $\mathbb{R}^d$, we need to face three difficulties, namely the unboundedness of the spatial domain, the appearance of Yukawa coupling terms γuv and $-\gamma|u|^2$ (nonlinear parts), and the conservation of the nonlocal energy. To overcome these three difficulties, we propose a linearized, energy-conserving, and adaptive time-stepping scheme by combining the Hermite-Galerkin spectral method with Crank-Nicolson/ESAV approach in this paper.

In particular, we find the proposed scheme enjoys the following three advantages compared with the classical schemes:

1) We utilize the Hermite-Galerkin spectral method to directly approximate the KGS system (1)-(4) in the unbounded domain, where the domain truncation and the establishment of artificial boundary condition can be avoided. When using other existing numerical methods to solve the problem in $\mathbb{R}^d$, however, one needs to i) truncate the unbounded domain to a bounded one which introduces additional errors and nonphysical singularities or ii) construct the artificial boundary condition which is highly nontrivial for fractional Laplacian.
2) We adopt the ESAV approach to deal with the Yukawa coupling terms explicitly. Thus, a linearly explicit and energy-conserving scheme is established by combining with the Crank-Nicolson method, which leads to the decoupled linear equations with constant coefficients. If one only uses the Crank-Nicolson method to construct linearly implicit conservative scheme for the problem, however, the resulting algebraic system involves variable coefficients which change at each time step.
3) We propose two kinds of time adaptive strategies to enhance the efficiency but without sacrificing accuracy of the scheme, where small (resp. large) time step size is adaptively selected if the time evolution of the system is quick (resp. slow). Numerical examples show that our time adaptive strategies are extremely efficient compared with the uniform time-stepping.

As the applications of the proposed scheme, the nonlinear interactions of vector solitons in two and three dimensional cases are successfully simulated to provide a deeper understanding of the Klein-Gordon-Schrödinger system. In addition, the scheme proposed in this paper can be extended to deal with other kinds of nonlocal conservative systems appearing in plasma physics, in optics, in water waves, etc.

Although ample numerical examples are provided in Sec. 4 to demonstrate the convergence order of the proposed scheme, we cannot establish the proof of the optimal error estimate. It is not clear whether the main difficulties lie in the intrinsic property of the KGS system (1)-(4) itself or in the limitation of the numerical analysis tools. This issue will be left as one of our future works.

CRediT authorship contribution statement

Shimin Guo: Conceptualization, Methodology, Software, Writing – original draft, Writing – review & editing. **Can Li:** Methodology, Writing – original draft, Writing – review & editing. **Xiaoli Li:** Methodology, Writing – review & editing. **Liquan Mei:** Supervision.

Declaration of competing interest

The authors declare that they have no known competing financial interests or personal relationships that could have appeared to influence the work reported in this paper.

Acknowledgements

The authors would like to express their sincere thanks to the anonymous reviewers for the constructive suggestions which greatly improved the quality of this paper.

References

[1] I. Fukuda, M. Tsutsumi, On coupled Klein-Gordon-Schrödinger equations, II, J. Math. Anal. Appl. 66 (2) (1978) 358–378.

[2] V. Makhankov, Dynamics of classical solitons (in non-integrable systems), Phys. Rep. 35 (1) (1978) 1–128.
[3] N. Laskin, Fractional quantum mechanics, Phys. Rev. E 62 (2000) 3135.
[4] N. Laskin, Fractional quantum mechanics and Lévy path integrals, Phys. Lett. A 268 (2000) 298–305.
[5] M. Jeng, S. Xu, E. Hawkins, J.M. Schwarz, On the nonlocality of the fractional Schrödinger equation, J. Math. Phys. 51 (2010) 062102.
[6] F. Pinsker, W. Bao, Y. Zhang, H. Ohadi, A. Dreismann, J.J. Baumberg, Fractional quantum mechanics in polariton condensates with velocity-dependent mass, Phys. Rev. B 92 (2015) 195310.
[7] A. Lischke, G. Pang, M. Gulian, et al., What is the fractional Laplacian? A comparative review with new results, J. Comput. Phys. 404 (2020) 109009.
[8] M. Sich, et al., Observation of bright polariton solitons in a semiconductor microcavity, Nat. Photonics 6 (2012) 50.
[9] B. Guo, Y. Li, Attractor for dissipative Klein-Gordon-Schrödinger equations in r^3, J. Differ. Equ. 136 (1997) 356–377.
[10] E. Compaan, Smoothing for the Zakharov and Klein-Gordon-Schrödinger systems on Euclidean spaces, SIAM J. Math. Anal. 49 (2017) 4206–4231.
[11] W. Bao, X. Dong, S. Wang, Singular limits of Klein-Gordon-Schrödinger equations to Schrödinger-Yukawa equations, Multiscale Model. Simul. 8 (2010) 1742–1769.
[12] W. Bao, L. Yang, Efficient and accurate numerical methods for the Klein-Gordon-Schrödinger equations, J. Comput. Phys. 225 (2007) 1863–1893.
[13] J. Hong, S. Jiang, C. Li, Explicit multi-symplectic methods for Klein-Gordon-Schrödinger equations, J. Comput. Phys. 228 (2009) 3517–3532.
[14] A. Riascos, J. Mateos, Fractional quantum mechanics on networks: long-range dynamics and quantum transport, Phys. Rev. E 92 (2015) 052814.
[15] T. Tang, L. Wang, H. Yuan, T. Zhou, Rational spectral methods for PDEs involving fractional Laplacian in unbounded domains, SIAM J. Sci. Comput. 42 (2020) A585–A611.
[16] H. Han, X. Wu, Artificial Boundary Method-Numerical Solution of Partial Differential Equations on Unbounded Domains, Tsinghua University Press, Beijing, 2009.
[17] H. Khosravian-Arab, M. Dehghan, M. Eslahchi, Fractional Sturm-Liouville boundary value problems in unbounded domains: theory and applications, J. Comput. Phys. 299 (2015) 526–560.
[18] H. Khosravian-Arab, M. Dehghan, M. Eslahchi, Fractional spectral and pseudo-spectral methods in unbounded domains: theory and applications, J. Comput. Phys. 338 (2017) 527–566.
[19] Z. Mao, J. Shen, Hermite spectral methods for fractional PDEs in unbounded domains, SIAM J. Sci. Comput. 39 (2017) A1928–A1950.
[20] S. Guo, L. Mei, C. Li, Z. Zhang, Y. Li, Semi-implicit Hermite-Galerkin spectral method for distributed-order fractional-in-space nonlinear reaction-diffusion equations in multidimensional unbounded domains, J. Sci. Comput. 85 (2020) 15.
[21] T. Tang, H. Yuan, T. Zhou, Hermite spectral collocation methods for fractional PDEs in unbounded domains, Commun. Comput. Phys. 24 (2018) 1143–1168.
[22] H. Ma, W. Sun, T. Tang, Hermite spectral methods with a time-dependent scaling for parabolic equations in unbounded domains, SIAM J. Numer. Anal. 43 (2005) 58–75.
[23] N. Landkof, Foundations of Modern Potential Theory, Springer, New York, 1972.
[24] J. Shen, J. Xu, J. Yang, The scalar auxiliary variable (SAV) approach for gradient flows, J. Comput. Phys. 353 (2018) 407–416.
[25] J. Shen, J. Xu, J. Yang, A new class of efficient and robust energy stable schemes, SIAM Rev. 61 (2019) 474–506.
[26] F. Huang, J. Shen, Z. Yang, A highly efficient and accurate new scalar auxiliary variable approach for gradient flows, SIAM J. Sci. Comput. 42 (2020) A2514–A2536.
[27] X. Li, J. Shen, Error analysis of the SAV-MAC scheme for the Navier-Stokes equations, SIAM J. Numer. Anal. 58 (2020) 2465–2491.
[28] Z. Liu, X. Li, The exponential scalar auxiliary variable (E-SAV) approach for phase field models and its explicit computing, SIAM J. Sci. Comput. 42 (2020) B630–B655.
[29] W. Chen, X. Wang, Y. Yan, Z. Zhang, A second order BDF numerical scheme with variable steps for the Cahn-Hilliard equation, SIAM J. Numer. Anal. 57 (2019) 495–525.
[30] Z. Qiao, Z. Zhang, T. Tang, An adaptive time-stepping strategy for the molecular beam epitaxy models, SIAM J. Sci. Comput. 33 (2011) 1395–1414.
[31] Y. Fu, W. Cai, Y. Wang, Structure-preserving algorithms for the two-dimensional fractional Klein-Gordon-Schrödinger equation, Appl. Numer. Math. 156 (2020) 77–93.
[32] Y. Fu, D. Hu, Y. Wang, High-order structure-preserving algorithms for the multi-dimensional fractional nonlinear Schrödinger equation based on the SAV approach, Math. Comput. Simul. 185 (2021) 238–255.
[33] J. Wang, A. Xiao, Conservative Fourier spectral method and numerical investigation of space fractional Klein-Gordon-Schrödinger equations, Appl. Math. Comput. 350 (2019) 348–365.
[34] Y. Wang, Q. Li, L. Mei, A linear, symmetric and energy-conservative scheme for the space-fractional Klein-Gordon-Schrödinger equations, Appl. Math. Lett. 95 (2019) 104–113.
[35] J. Shen, T. Tang, L.L. Wang, Spectral Methods: Algorithms, Analysis and Applications, Springer Ser. Comput. Math., vol. 41, Springer, Heidelberg, 2011.
[36] W. Gautschi, Orthogonal Polynomials: Computation and Approximation, Numer. Math. Sci. Comput., Oxford University Press, New York, 2004.
[37] Y. Saad, M.H. Schultz, GMRES: a generalized minimal residual algorithm for solving nonsymmetric linear systems, SIAM J. Sci. Stat. Comput. 7 (1986) 856–869.
[38] H. Gomez, T. Hughes, Provably unconditionally stable, second-order time-accurate, mixed variational methods for phase-field models, J. Comput. Phys. 230 (2011) 5310–5327.
[39] Q. Li, N. Wang, D. Yi, Numerical Analysis, 5th edition, Tsinghua University Press, Beijing, 2008.
[40] C. Huang, B. Guo, D. Huang, Q. Li, Global well-posedness of the fractional Klein-Gordon-Schrödinger system with rough initial data, Sci. China 59 (2016) 1345–1366.
[41] F. Zeng, I. Turner, K. Burrage, G. Karniadakis, A new class of semi-implicit methods with linear complexity for nonlinear fractional differential equations, SIAM J. Sci. Comput. 40 (2018) A2986–A3011.
[42] J. Zhang, Numerical methods for nonlocal and anomalous diffusion models, J. Numer. Methods Comput. Appl. 42 (2021) 183–214.